NTNU
Norwegian University of
Science and Technology

Position Control in Inductive Power Transfer

Kristian Holmstrøm

Master of Science in Industrial Cybernetics
Submission date: January 2018
Supervisor: Marta Maria Cabrera Molinas, ITK

Norwegian University of Science and Technology
Department of Engineering Cybernetics

Position Control in Inductive Power Transfer

Kristian Holmstrøm

January 18, 2018

Problem Description

Investigate the use of position control in inductive power transfer, and how it compares to state-of-the-art methods for inductive power transfer control.

Acknowledgments

I thank prof. Marta Molinas for her help and guidance on this thesis.

I also would like to thank my sister for her input and creativity, as well as my father for helping me solve some especially gnarly elliptic integrals.

Abstract

English

The objective of this thesis has been to investigate the use of position control in inductive power transfer and how it compares to the state-of-the-art methods for inductive power transfer control.
In this thesis we have:

- Outlined the basic principles for the design and control of IPT systems for high power applications
- Calculated magnetic field for a thin circular coil and mutual inductance between two thin circular coils
- Calculated transfer functions for SS compensated IPT systems for CR and CV load
- Demonstrated position control for lateral and axial displacement of the receiving coil relative to the transmitter

The use of position control to keep the mutual inductance constant and thus optimize the efficiency of an IPT system has been investigated. With operations in the nearfield region, the mutual inductance is highly volatile, both for axial and lateral movement. Maintaining a constant reference position in this region imposes demanding requirements on both the controlling unit and the mechanical apparatus responsible for the physical movement. The farfield operation, however, is more forgiving.

Complete system analysis has to be done for each specific implementation, as the inertia of the system and the input dynamics must be known. The added cost of implementing and maintaining such a system needs to be considered. It is argued that for most high power applications, the state-of-the art solution is better for most high power applications. Tight position control may still have its niche applications.

Future work in this field, need to consider a specific application in order to get reliable information regarding the most important parameters: position measurements, actuators and life-cycle costs. Another line of future work is to continue the work of modelling the mutual inductance for general relative movement and try to find approximative solutions that can be used for simpler design of new systems.

Norwegian

Målet med denne oppgaven har vært å undersøke bruken av posisjonskontroll i induktiv kraftoverføring og hvordan det sammenlignes med de nyeste metodene for induktiv kraftoverføringskontroll.
I denne oppgaven er det:

- Skildret de grunnleggende prinsippene for design og kontroll av IPT-systemer for høyeffektapplikasjoner
- Beregnet magnetfelt for en tynn sirkulær spole og gjensidig induktans mellom to tynne sirkulære spoler
- Beregnet overføringsfunksjoner for SS-kompenserte IPT-systemer for CR og CV-last
- Demonstrert posisjonskontroll for lateral og aksial forskyvning av mottaker spolen i forhold til sender spolen.

Bruk av posisjonskontroll for å holde gjensidig induktans konstant og dermed optimalisere effektiviteten til et IPT-system er blitt undersøkt. Med operasjoner i nærområdet, er den gjensidige induktansen svært volatil, både for aksial og lateral bevegelse. Ved å opprettholde en konstant referanseposisjon i denne regionen stilles strenge krav til både kontrollenheten og det mekaniske apparatet som er ansvarlig for den fysiske bevegelsen. Fjærnfeltoperasjonen er imidlertid mer tilgivende.

Fullstendig systemanalyse må gjøres for hver spesifikk implementering, da tregheten til systemet og inngangsdynamikken må være kjent. Den ekstra kostnaden ved å implementere og vedlikeholde et slikt system må vurderes. For de fleste høyeffektapplikasjoner er andre moderne løsninger sannsynligvis bedre for de fleste applikasjoner med høy effekt. Posisjonskontroll kan fortsatt ha sine nisjeprogrammer.
Fremtidig arbeid på dette feltet må se spesifikt på en bestemt applikasjon for

å få pålitelig informasjon om de viktigste parameterne: posisjons målinger, aktuatorer og livssykluskostnader. En annen retning for fremtidig arbeid er å viderføre arbeidet med å modellere den gjensidige induktansen for generell relativ bevegelse og forsøke å finne approksimative løsninger som kan brukes til enklere design av nye systemer.

Contents

List of Figures

List of Tables

Chapter 1

Introduction

Wireless inductive power transfer, IPT for short, is a technology where electric power is wirelessly transferred between two coils. The concept has a long history and was demonstrated by Nicola Tesla himself, in the beginning of the 20^{th} century (3) . Though, due to the technological limitations of the era, price vs. efficiency and lack of means to regulate the process, the prospect of wireless energy transfer looked bleak, and interest in further investigation quickly waned.

Now, at the beginning of the 21^{st} century, with a century's worth of technological advancements past, IPT is back with a vengeance. The first use of IPT has been in applications such as industrial automation, medical implants, security system, clean rooms and consumer electronics (portable electronic devices) where the power requirements are relatively low and where transmitter and receiver can be brought relatively close (13; 3). However, it is especially the last few years' rise in electrical vehicles populating the roads which has ushered a focus on using and improving IPT, to deliver power to batteries wirelessly. Ambitions stretch from designing stationary wireless charging system unaffected by chemicals, dirt or weather, to the seemingly more daunting task of dynamically charging a moving vehicle along the road.

Even with the advancements of technology, there are certain physical characters of the IPT technology which will limit the energy transfer efficiency. For existing low energy solutions such as wireless mobile phone charging, a 10-30 % energy loss is acceptable. However, for high energy applications such as vehicle battery charging, even a 10 % energy loss is substantial and unfavorable. Carefully designing specifically variables such as the positioning between sending and receiving coils, resonance frequencies and circuit and magnetic design will determine efficiency and usability of the system in prac-

tical applications (5). Thus, efforts have to be made to develop high energy wireless IPT systems, which reduces the transmission energy dissipation to acceptable levels. For high power applications with loose coupling (medium to long relative distance) between transmitter and receiver, capacitive compensation networks are necessary in order to compensate for the reactive losses caused by low magnetic coupling.

The objective of this thesis is to investigate the use of position control in inductive power transfer and how it compares to the state-of-the-art methods for inductive power transfer control. IPT system are designed for a specific nominal distance between transmitter, and careful selection of components, magnetic design, rectifiers and switching power supply are needed in order to minimize losses and maximize system throughput. Once the IPT system has been designed, any relative movement between transmitter and receiver will move the system from its optimum. In order to bring the system back close to optimal operation, there are only three possible ways to control a basic IPT system: increase transmitter current, increase the operating frequency or controlling the magnetic coupling between transmitting and receiving coils.

In this thesis, the control of influence on transmission efficiency of the relative position between coils is investigated in detail and the behavior and challenges with a position regulated IPT system will be demonstrated. Specifically, this work makes the following contributions:

- Systematic presentation of the basics of IPT circuit design and behavior in chapter 2
- Establish how the magnetic coupling varies with distance and misalignment in chapter 3
- In chapter 4, derivation of transfer functions for a series-series (SS) compensated IPT systems, which demonstrates challenges in system design
- In chapter 5, through Matlab system modelling and simulations, demonstration of the influence of coil positioning on the coupling coefficient, how this further effects transmission efficiency, and how a position regulator can be used to ensure optimal energy transmission.
- Discussion about the practical applicability of position control as a mean to stabilize power transfer in IPT systems

Three appendices are included: In appendix A a detailed derivation of some of the results about magnetic field and mutual inductance are given. Appendix B contains a detailed derivation of the frequency response for a SS compensated IPT system

Chapter 2

Background

This chapter will touch on a few topics central to inductive power transfer. Individual components and phenomena of importance are explained, as well as how they interact with each other. The aim is to have a basic understanding of how a IPT operates, common design differences, and what the biggest obstacles to overcome are.

In chapter 2.1 we give an introduction to the basic of controlling an IPT system. The basic circuits design for resonant energy transfer is explained in chapter 2.2 and the relation between circuit design and mutual inductance is discussed in chapter 2.3. In chapter 2.4 the system characteristics of an IPT system are discussed: Operational mode, topology and bifurcation. The often conflicting factors to consider in order to maximize output power is considered in chapter 2.5. Achieving stable output power through control is the topic of chapter 2.6.

The two most important papers for this chapter is ((18; 17)). However, there are a number of papers available with a good overview of wireless power transfer and its applications (Barman et al. (3); Covic and Boys (11); Brecher and Arthur (7); Fernández et al. (13); Li and Mi (22)),and quite a few that dig into the details on optimised design of IPT systems both in general and for specific applications (Bosshard et al. (5); Wang et al. (29); Steigerwald (26); Diekhans and Doncker (12); Boys et al. (6); Wang et al. (30); Garnica and Lin (16); Kurs (21); Mur-Miranda et al. (23)).

2.1 Introduction

There are two simple and interrelated physical principles that forms the basis for wireless power transfer:

A current in a wire produces a magnetic field that permeates the volume around it.

and

A surface enclosed by a wire exposed to a time-varying magnetic field will generate a voltage in the wire.

Like a transformer, the basic principle behind inductive power transfer is to use a primary electric circuit to generate a magnetic field, which in turn induces a voltage in a secondary electric circuit away from the primary circuit. The problem is that we want to transfer energy over some distance, and unlike a transformer the coupling between the primary and secondary circuit may be low.

The maximum power that can be drawn from the secondary circuit is in most application not sufficient. In order to increase the maximum power output, a capacitor is added in the pickup circuit, and the system is operated in resonance with the primary circuit. It has been shown ((6)) that in resonance the maximum output power is:

$$P_{out} = \omega I_1^2 \frac{M^2}{L_2} Q \tag{2.1}$$

Here ω is the operating frequency and I_1 is the current in the primary circuit. M is the mutual inductance, which is a function of the relative distance between the two coils. L_2 is the inductance in the pickup circuit and Q is the tuned quality factor. The equation captures the basic challenges with IPT and controlability, and eq. 2.1 will be discussed in detail in later chapters.

As mentioned in the introduction chapter, for applications where there is relative movement between the two coils, it is necessary to apply some sort of control if the system is required to maintain a stable output power. In order to be able to quantify the requirements for the controller, some background info on the basic IPT system design elements and considerations is given in this chapter, and the basic concept of mutual inductance is disclosed. When this information has been established, it is shown, with reference to

equation 2.1, how a stable output power can be achieved either through input frequency regulation or relative position control between the two coils. Furthermore, the level of which the different variables as given in equation 2.1 can be tuned to maximize the output power is succinctly given.

2.2 IPT fundamentals

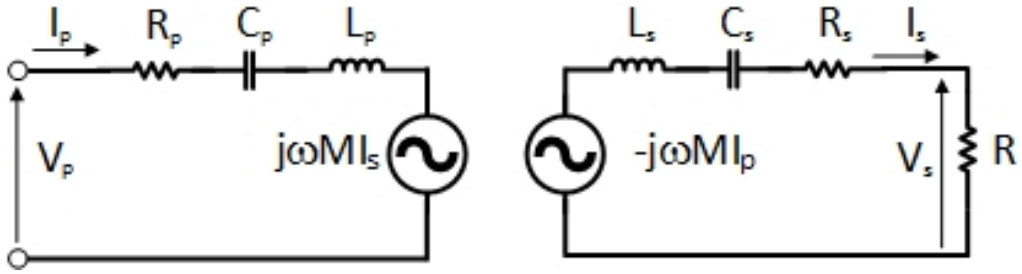

Figure 2.1: Basic Circuit Model

In its most rudimentary form, an inductive power transfer (IPT) system consist of a *primary* (sending, transmitter) circuit, and a *secondary* (pickup, receiver) circuit, as shown in figure 2.1 for a SS topology (see 2.4 for possible topologies)

Each circuit usually consists of a resistance, inductance and a capacitance. The resistance in the primary circuit, R_p, represents the resistance in the circuit that causes unwanted ohmic losses.The secondary circuit is often modeled with two resistances; R_s is the resistance in the secondary circuit that results in unwanted ohmic losses, and R_L is the load resistance . When analyzing lossless cases, the values of the intrinsic resistances, R_p and R_s, are zero:

$$R_p = R_s = 0 \tag{2.2}$$

The load resistance, often denoted R_L or R_{eq} varies greatly with the design of the system. This is the reason it is preferable to express additional complexity of the circuit through the load.

When power is applied to the primary circuit, the current i_p will generate an electromagnetic field which varies with a frequency ω_p. This is the same frequency as that of the applied source voltage/current. IPT's usually operate in the $kHz - GHz$ range, which is one of the reasons frequency converters are used for making sure that the input current/voltage has the desired frequency. Being able to alter this frequency ω_p, makes it possible to tune it to the primary circuits own frequency ω_0. The primary circuits resonance frequency is defined as:

$$\omega_0 = \frac{1}{\sqrt{C_p L_p}} \tag{2.3}$$

If the applied power has a frequency that is equal to the circuit's resonance frequency, the power will be transferred from the source to the end of the circuit without any reactive losses. The same holds for the secondary circuit if its inductance and capacitance is tuned to a frequency equal ω_0.

In addition to these beneficial characteristics, the air gap between the two coil is a critical part of an IPT, with a lot of nuances on how to bridge the divide between the two coils. Knowledge on the next topic of mutual inductance is vital for understanding the influence of the air gap between and position of the two coils.

2.3 Mutual Inductance

When an electromagnetic field generated by a coil is picked up by another adjacent coil, the two coils are linked together by a common magnetic flux; they share a mutual inductance between them. With no losses the mutual inductance is:

$$M = \sqrt{L_P * L_S} \tag{2.4}$$

This is for zero flux leakage and perfect coupling, which is more applicable for transformers than for IPT, where distance and/or orientation between the coils result in a change in the amount of magnetic flux the two coil shares between them. For IPT, the coefficient "k" describes the "state" of the inductive coupling between the two coils. It is defined as:

$$k = \frac{M}{\sqrt{L_P * L_S}}, k \in [0, 1] \tag{2.5}$$

The coupling coefficient is usually expressed as a decimal value although percentage is occasionally used. A rearrangement gives the common expression for mutual inductance, used for IPT:

$$M = k\sqrt{L_P L_S} \tag{2.6}$$

What can be seen from equation 2.6 is that in order to have high mutual inductance, large quality coils are important.

Furthermore, we see that the coupling coefficient has more influence on the mutual inductance than the coil selection. The coupling coefficient is strongly connected to the relative distance and orientation between the two coils. The figure below illustrates the three spatial degrees of freedom that affects the coupling coefficient of the system. The exact relationship between the coupling coefficient and the displacement is a complex subject, that requires an analysis of the magnetic field strength and shape. This will be covered in Chapter 3 and Appendix A.

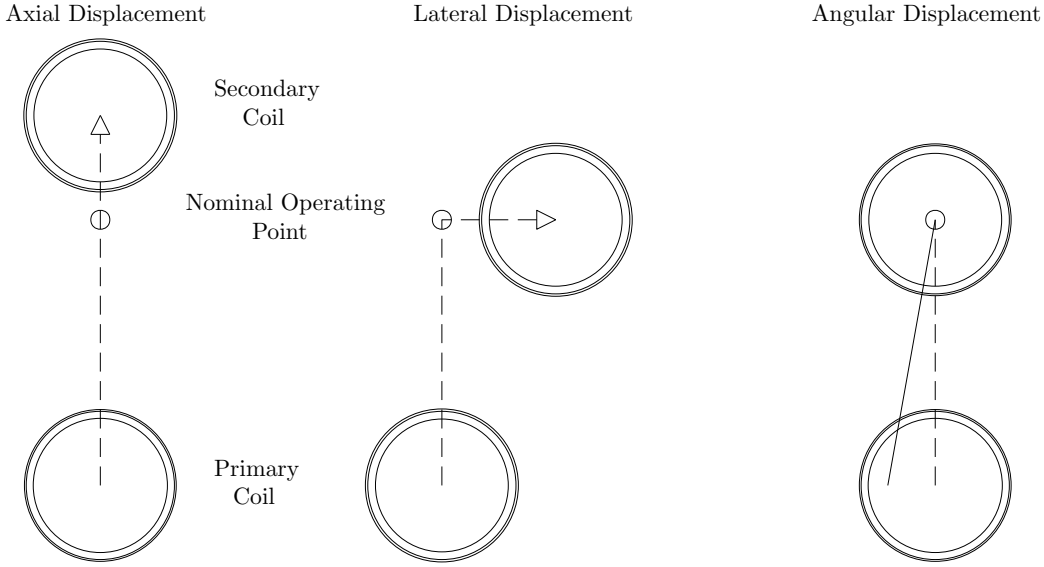

Figure 2.2: Three Cases of Displacement

2.4 System Characteristics

2.4.1 Configurations

There are two main types of configurations in an IPT system; *constant resistance (CR)* and *constant voltage (CV)*. The constant resistance model is used when the load is purely resistive. In a lot of IPT applications, power is delivered wirelessly to a battery, where maintaining a stable rated voltage is in focus. Hence, for such systems constant voltage load is the applicable model.

Table 2.1: Topology Key Metrics

Configuration	Series	Parallel
Secondary impedance $[Z_s]$	$j\omega L_s + \frac{1}{j\omega C_s} + R$	$j\omega L_s + \frac{1}{j\omega C_s + \frac{1}{R}}$
Load Voltage $[V_L]$	$I_s R$	V_s
Load current $[I_L]$	I_s	$\frac{V_s}{R}$
Reflected resistance	$\frac{\omega_0^2 M^2}{R}$	$\frac{M^2 R}{L_s^2}$
Reflected reactance	0	$-\frac{\omega_0 M^2}{L_s}$
Secondary Quality factor $[Q_s]$	$\frac{\omega_0 L_s}{R}$	$\frac{R}{\omega_0 L_s}$

2.4.2 Topology

The topology of an IPT system is the arrangement of the components in the system. The topology can be complex, but will usually be a combination of only four basic configurations. There are no clear best alternative, as each configuration have different advantages and drawbacks. The four basic ones are:

- Series - Series [SS]
- Series - Parallel [SP]
- Parallel - Series [PS]
- Parallel - Parallel [PP]

According to (26) the correct topology are dependent on the constraints imposed on the system. Series configuration on the primary side allows for a lower primary voltage, while a parallel configuration gives a high primary current. On the secondary side a series configuration gives stable voltage while a parallel setup gives a stable current. Table 2.1 shows some key properties of the secondary side with different topology configurations.

It is important to note that some of the unwanted effects accompanying a topology can be resolved using different techniques. An example of this is canceling out the reflected reactance of a secondary parallel configuration by tuning it out, because it is independent of the load.(30)
The quality factor for the configurations are shown in table 2.2 (29). The Q-factor plays a big part in the magnetic losses in the circuit, and as such the overall efficiency of the system. We will come back to this later when

Table 2.2: Q-factor Topologies

	Q_P	Q_S
Series Secondary	$\frac{L_P R}{\omega_0 M^2}$	$\frac{\omega_0 L_S}{R}$
Parallel Secondary	$\frac{\omega_0 L_P L_S^2}{M^2 R}$	$\frac{R}{\omega_0 L_S}$

discussing efficiency. For now just note that the component values relates to the Q-factor quite differently for the two configurations, and as such must be carefully considered.

2.4.3 Bifurcation

Bifurcation is generally described as a topological change in system behaviour, caused by a small smooth change in the parameters of the system. In IPT, bifurcation manifests itself when a small change in system parameters results in the system going from having a singular resonant frequency to having three resonant frequencies. In (29) it is shown how careful design for the different topologies can avoid bifurcation, see table 2.3. The result for a SS compensated topology has also been derived in appendix B,

Table 2.3: Q-factors to avoid bifurcation

SS	$Q_P > \frac{4Q_S^3}{4Q_S^2-1}$
SP&PP	$Q_P > Q_S + \frac{1}{Q_S}$
PS	$Q_P > Q_S$

However, it is possible to take advantage of the bifurcation phenomena as described in (18) where an unbalancing factor "x_u" defined as:

$$x_u^2 = \frac{L_p}{L_s}\Big(\frac{V_s}{V_p}\Big)^2 \tag{2.7}$$

An unbalancing of "x_u" >1 may be added in order to prevent bifurcation. However, it may instead purposely designed with "x_u" values < 1. This results in a small degree of bifurcation with the two additional resonance tops moving away from one another. The frequency band between the two of them is still one of high efficiency. In (5) they found the drop in efficiency not to be significant as long as the unbalancing is kept within $10 - 20\%$.

This allows for a system with high efficiency over a larger range of coupling conditions.

2.5 Efficiency: Maximum output power

The efficiency of a SS configuration shown in the figure 2.1is:

$$\eta = \frac{i_2^2 R_L}{i_1^2(R_S + R_p) + i_2^2(R_s + R_L)} \tag{2.8}$$

From 2.8 it is evident that reducing the source and primary impedance, will yield a better efficiency. We can rewrite 2.8 and express it in terms of "Q" and "k" (22):

$$\eta_{max} = \left(\frac{k * Q}{1 + \sqrt{1 + (k * Q)^2}} \right)^2 \tag{2.9}$$

This equation explains how alignment affects the efficiency through "k" and can according to (22) be viewed as a general formula to gauge power transfer efficiency, as it is valid for multiple forms of compensation networks. Figure 2.3 shows a plot of a select values of Q and k. If the value for "k" is too

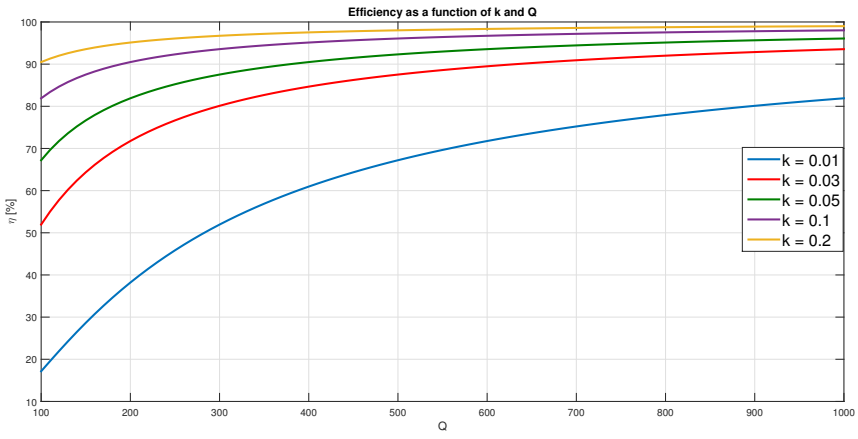

Figure 2.3: Efficiency as a function of Q and k

low, the drop in efficiency is substantial, and would need a really high Q to compensate. This are considerations done during the design of the system. Another aspect is the operation of the system. As stated earlier the coupling might change during operation, and this will impact the efficiency of the system as less power will be transferred over the link. As such this

needs to be compensated, so that rated power can be delivered to the load. From equation 2.1 with equal inductance's on primary and secondary side ($L_p = L_s$) it can be expressed as:

$$P_{out} = \omega \times k^2 \times L \times I_1^2 \times Q_2 \tag{2.10}$$

We see from the equation 2.10 that given a 50 % drop in coupling coefficient we can compensate by either:

- increase the frequency to 400 % of nominal value
- increase the primary current to 200 % of nominal value
- increase the secondary quality factor to 400 % of nominal value

Increasing the primary current is the last resort, since it will maintain the rated output power, but it will also put more stress on all the components as well. As such the solution usually leads to a lower efficiency.

Increasing the frequency might seem like a good idea, but the frequency dependency is more complex than equation 2.10 reveals, and it might not bring about the benefits expected.

Increasing the quality factor of the secondary circuit is a good solution, but this compensation has it's limits. Increasing it too much will narrow the operating bandwidth, and as a result the system will be difficult to tune correctly as well to re tune over time as component decay affects the nominal operating frequency.

The ideal solution is to maintain the coupling coefficient, as the only drawback is the investment cost in making the magnetics better and the increase in volume.(10)

The coupling coefficient variations during operation, sets the VA rating on the input converter. Mathematically:(29)

$$S_p \approx \frac{k_{max}}{k_{min}} \times P_{rated} \tag{2.11}$$

As such minimizing the coupling coefficient variations, allows for lowering the rating of the converter, and as such the price of the system.

As mentioned earlier a high quality factor of the secondary circuit increases the output power. Systems with a fixed frequency, closely matching the VA ratings of the primary and the secondary circuits, provides normally the best operating condition(10). The largest lateral displacement at maximum VA rating tolerated is:

$$k \times Q_s \approx 1 \tag{2.12}$$

Equation 2.12 shows that a large quality factor of the secondary circuit, increases the lateral offset tolerated. There is however a catch as the magnetic losses of both primary and secondary at rated power are proportional to Q_s/Q_L (Takanashi et al.) . Q_L is the native Q-factor of the inductor:

$$Q_L = \frac{\omega L}{r_{ac}} \tag{2.13}$$

, where r_{ac} is the intrinsic resistance of the wire in the coil at the operating frequency.
Another expression for Q_L is:

$$Q_L = \frac{\omega}{BW} \tag{2.14}$$

Here BW is the bandwidth of the tuned circuit. With this relation, it is clear that in order to increase the output power by increasing Q_s, Q_L has to be high as well. This keeps the magnetic losses low, but also decreases the transfer bandwidth, making tuning increasingly difficulty as Q_L is raised.

2.6 Control and stability of output power

Equation 2.1 gave the relationship between output power and different system variables as:

$$P_{out} = \omega I_1^2 \frac{M^2}{L_2} Q = a \cdot b \tag{2.15}$$

Where $a = \omega I_1^2$ and $b = \frac{M^2}{L_2} Q$. There are in principle two methods that can be used for maintaining a stable output power when the relative position varies:

a. Vary the frequency and/or the magnitude of the current in the primary circuit $\rightarrow$ using a to compensate for changes in b due to position variation.

b. Eliminating the variations in the mutual inductance by control of the relative position between the two coils $\longrightarrow$ keeping a constant, directly regulate the position to ensure b is as close to constant as possible.

a. Vary input frequency or - current. As mentioned in the introduction, the method of regulating the output power by mean of input circuit frequency control, is by far the most promising method, and multiple systems have been proposed.

Giuseppe Guidi and Jon Are Suul have developed a method for minimizing the rating requirements of power electronic converters in IPT systems intended to transfer rated power over a wide range of coupling conditions. The increased operating range is achieved by designing the coils with a small unbalance factor, compared to the ideal and well-known conditions of perfectly matched load, resulting in operation at rated load that is beyond the bifurcation limit of the system. The global ZVS(Zero Voltage Sum) conditions at rated power is ensured by slightly detuning the resonant frequencies of both primary and secondary coils. The method is experimentally demonstrated for coupling variations as high as 275 % Guidi (17); Guidi and Suul (18).

b. Position Control. The focus in this work, the latter method using position control, is quite straightforward and well known - at least when the masses involved are small and the needed accelerations and forces are not too high.

2.7 Summary

In this chapter the basic circuit design of WPT systems have been shown, together with the different configurations that can be used to obtain different overall system characteristics. Furthermore, the basic concept of mutual inductance was given, and it was shown how the mutual inductance varies with the coupling coefficient k, which in turn varies with the relative position between sending and receiving coils in the WPT systems. Lastly, the output power and its relationship to the relative position was discussed, and two methods for ensuring a stable output power in presence of varying position was given.

The method of directly controlling the relative position is the method to be implemented here. Before this can be done, the concept of mutual inductance and how it relates to the position through k will be derived subject

to sound assumptions. This is necessary to be able to design a plausible controller, and demonstrates in detail the complexity of position control in WPT systems.

Subsequently, the transfer functions for specific IPT system configurations, some of which ares given in Guidi (17); Guidi and Suul (18), are derived in order to set up the system model correctly, and to be able to directly compare performance with their method. Additionally, the response using the derived relationships is compared to the responses as given by Guidi and Suul, supporting their findings.

Chapter 3

Magnetic field and coupling

In order to control the mutual inductance when position changes, we need to know how the mutual inductance and the magnetic field varies with the relative orientation of two coils. A general discussion about the magnetic field from realistic transmitter, requires detailed modelling of a specific magnetic configuration which is beyond the scope of this master thesis. In order to get an understanding on how the magnetic field and mutual inductance varies with position, we choose to study one of the simplest IPT arrangement, that of two circular thin wire coils.

This chapter presents a summary of the theory and formulas used for calculating magnetic field and mutual inductance. In appendix A, a much more detailed description is given. In 3.1, mutual inductance and the coupling coefficient are defined and a summary of formulas and methods for calculating the magnetic field and mutual inductance is given. In section 3.2 the magnetic field from a circular loop is calculated. The mutual inductance between two circular loops is derived in section 3.3 for two coil arrangement with circular coils. The first one is for two coaxial circular loops and for the second arrangement the receiving coil is displaced from the symmetry axis of the transmitter coil.

3.1 Mutual inductance and coupling coefficient

Let Γ be a curve in space enclosing a surface Ω, and let $\vec{\boldsymbol{B}}(\vec{r}, t)$ be the magnetic field through that surface. The magnetic flux through the surface is defined as:

$$\Phi(t) = \int_{\Omega} \vec{\boldsymbol{B}}(\vec{r}, t) \cdot \vec{\boldsymbol{dS}} \tag{3.1}$$

If the curve Γ represents an electric circuit, the electromotive force (emf) generated in the circuit is:

$$\varepsilon(t) = -\frac{d\Phi(t)}{dt} \tag{3.2}$$

This is Faraday's law, which states that if the magnetic field, or the enclosed surface is time-varying, a voltage is generated that opposes the change in the magnetic flux.

A closed electric loop will, as will be shown later, generate a magnetic field. Since the loop encloses a surface, it will experience a flux and emf due to the field it has generated. If I is the current through the circuit, the emf generated by self induction is:

$$\varepsilon(t) = -L\frac{dI(t)}{dt} \tag{3.3}$$

where L is the self inductance. This is of course the standard equation for an inductance, and L depends on the characteristics of the material and the frequency used.

Now assume we have two circuits in proximity to each other, with current I_a and I_b respectively, and let L_a and L_b be the corresponding inductances. We can now write:

$$\varepsilon_A(t) = L_A\frac{dI_A}{dt} + M_{BA}\frac{dI_B}{dt} \tag{3.4}$$

$$\varepsilon_B(t) = L_A\frac{dI_B}{dt} + M_{AB}\frac{dI_B}{dt} \tag{3.5}$$

where M_{AB} is the mutual inductance between the two circuits. Due to symmetry, the two mutual inductances has to be equal:

$$M = M_{AB} = M_{BA} \tag{3.6}$$

By considering the total magnetic energy of the system, it can be shown that M, L_A and L_A has to satisfy the inequality (14):

$$M^2 \leq L_A L_B \tag{3.7}$$

Introducing the coupling coefficient, the relation between the mutual inductance and the self-inductances may be defined as

$$M = k\sqrt{L_A L_B} \tag{3.8}$$

where k is the coupling coefficient which varies between 0 and 1. The coupling coefficient and the mutual inductance contains all the information about the magnetic coupling between the two circuit, and how the coupling between the two circuits varies with the relative distance between the two circuits. In order to evaluate if control is viable, we need to find a process model which in our case is the mutual inductance.

3.1.1 Calculating magnetic fields and mutual inductance

The magnetic flux and the mutual inductance may be calculated in various ways, and the starting point for calculations varies a lot in the literature. Our approach is to calculate the flux through the receiver loop by evaluating

$$\Phi(t) = \oint_{\Gamma_2} \vec{\boldsymbol{A}}(\vec{r}, t) \cdot \vec{\boldsymbol{dl}} \tag{3.9}$$

to calculate the flux through a surface enclosed by a curve Γ_2 which represents our receiver loop. Here $\vec{\boldsymbol{A}}(\vec{r}, t)$ is the vector potential produced by the source loop:

$$\vec{\boldsymbol{A}}(\vec{r}, t) = \frac{\mu_0}{4\pi} \int_V \frac{\vec{\boldsymbol{j}}(\vec{r}_0, t)}{|\vec{\boldsymbol{r}} - \vec{\boldsymbol{r}}_0|} d^3 r_0 \tag{3.10}$$

where V is the volume of the source loop and $\vec{\boldsymbol{j}}(\vec{r}_0, t)$ is the current density throughout the volume. If we can find an expression for the vector potential, the magnetic field $\vec{\boldsymbol{B}}(\vec{r}, t)$ can be found relatively easy through

$$\vec{\boldsymbol{B}}(\vec{r}, t) = \nabla \times \vec{\boldsymbol{A}}(\vec{r}, t) \tag{3.11}$$

So far, no approximations has been made and eq. 3.9-3.11 is the equations to be used (numerically) for complex geometries for source and/or receiver circuits.

Thin wire approximation We will in this thesis only consider wires carrying a current I where the shape and dimension of the cross section is very

small compared to the length of the wire. It is shown in appendix A that with this approximation the vector potential is:

$$\vec{\boldsymbol{A}}(\vec{r},t) = \frac{\mu_0 I(t)}{4\pi}\int_\Gamma \frac{1}{|\vec{\boldsymbol{r}}-\vec{\boldsymbol{r}}_0|}\vec{\boldsymbol{dl_0}} \tag{3.12}$$

where $\vec{\boldsymbol{dl_0}}$ is a line element tangential to the wire. The obvious advantage is that we have replaced a volume integral with a line integral along the wire. The disadvantage is that the resulting integral is singular on the wire, and the results is not valid close to the source loop. We will not consider this further in this thesis.It should be observed from eq. 3.12 that the time dependency of $\vec{\boldsymbol{A}}(\vec{r},t)$ is only through the current $I(t)$ which makes it very easy to find the mutual inductance once the flux is known.

3.2 Magnetic field from circular loop

In the rest of this chapter we will consider a circular loop both as source and receiver circuit.

3.2.1 Vector potential

First we consider a circular wire in the xy-plane with center at (0,0,0) and radius a, carrying a current I. It is shown in appendix A that the vector potential from this wire in a position (ρ, z) is:

$$\vec{\boldsymbol{A}}(\vec{r}) = \frac{\mu_0 I a}{\pi\sqrt{(\rho+a)^2+z^2}}\frac{(2-m^2)K(m)-2E(m)}{m^2}\vec{\boldsymbol{e_\theta}} \tag{3.13}$$

where K(m) and E(m) are complete elliptic integrals of first and second kind, and where we have defined

$$m^2 = \frac{4\rho a}{(\rho+a)^2+z^2} \tag{3.14}$$

The vector potential in a point has direction tangential to a circle with center on the symmetry axis and through the point.

3.2.2 Magnetic field

The magnetic field may be calculated from the vector potential $\vec{\boldsymbol{A}}(\vec{r})$ by using 3.11. The results in cylindrical coordinates is:

$$B_\rho(\rho,z) = \frac{Cz}{2\alpha^2\beta\rho}[\frac{\alpha^2+\beta^2}{2}E(m)-\alpha^2K(m)] \tag{3.15}$$

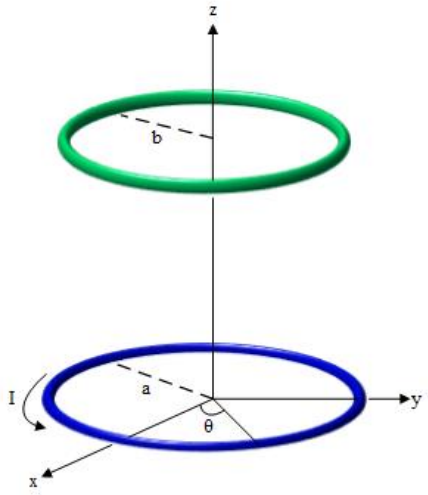

Figure 3.1: Coil arrangement for two coaxial circular loops

$$B_z(\rho, z) = \frac{C}{2\alpha^2\beta}[\alpha^2 K(m) + (a^2 - \rho^2 - z^2)E(m)] \tag{3.16}$$

where

$$C = \frac{\mu_0 I}{\pi} \tag{3.17}$$

$$\alpha^2 = (a - \rho)^2 + z^2 \tag{3.18}$$

$$\beta^2 = (a + \rho)^2 + z^2 \tag{3.19}$$

$$m^2 = \frac{4a\rho}{(a + \rho)^2 + z^2} = 1 - \frac{\alpha^2}{\beta^2} \tag{3.20}$$

The axial field (in the z-direction) for a circular loop as a function of distance from the symmetry axis is shown in Figure 3.2 for distances not too far from the loop. It is seen that close to the plane of the current loop the axial field changes rather abruptly close to the wire. Furthermore, the magnetic field switches direction from the positive z-direction to the negative. The distance from the axis where the change of direction happens is $\rho = a$ at the

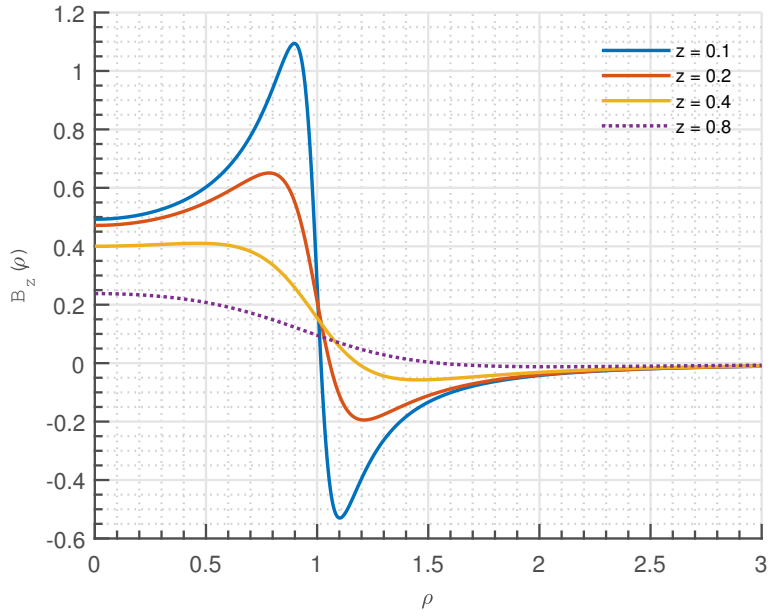

Figure 3.2: Axial magnetic field as a function of distance from the symmetry axis for 4 distances along the axis: $z = 0.1a, 0.2a, 0.4a$ and $0.8a$

wire plane, and increases the further away from the axis one moves. If we consider the magnetic flux through another coaxial circular shaped wire loop in a plane parallel to the xy-plane, it will be positive. However, if we move this coil further and further away from the axis in the near field the flux will at some distance become negative.

The axial field (in the z-direction) further away from the loop plane is shown in Figure 3.3. It is seen that the magnetic field changes more smoothly with distance from the axis, but it still becomes negative some distance from the axis.

The radial field is shown in Figures 3.4 and 3.5 for the same distances as for the axial field. For distances close to the loop, the radial field is sharply peaked around $\rho = a$ and above.

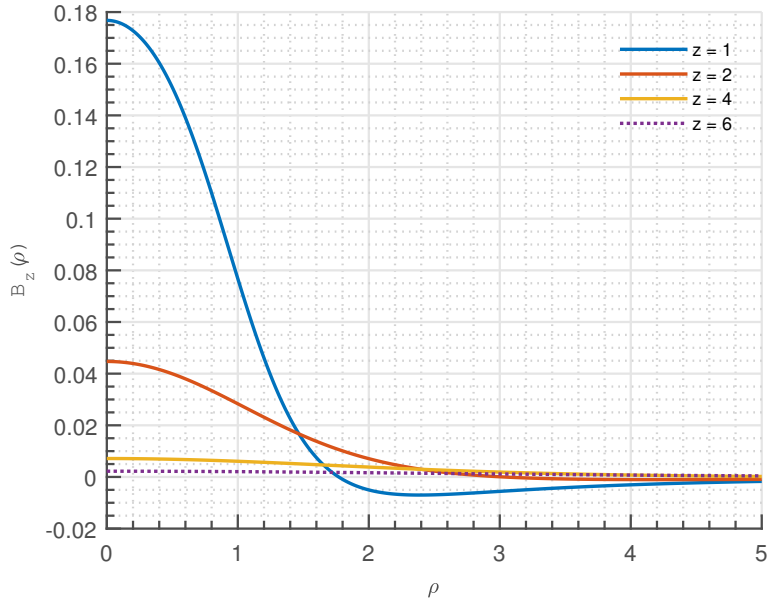

Figure 3.3: Axial magnetic field as a function of distance from the symmetry axis for 4 distances along the axis: $z = a, 2a, 4a$ and $6a$

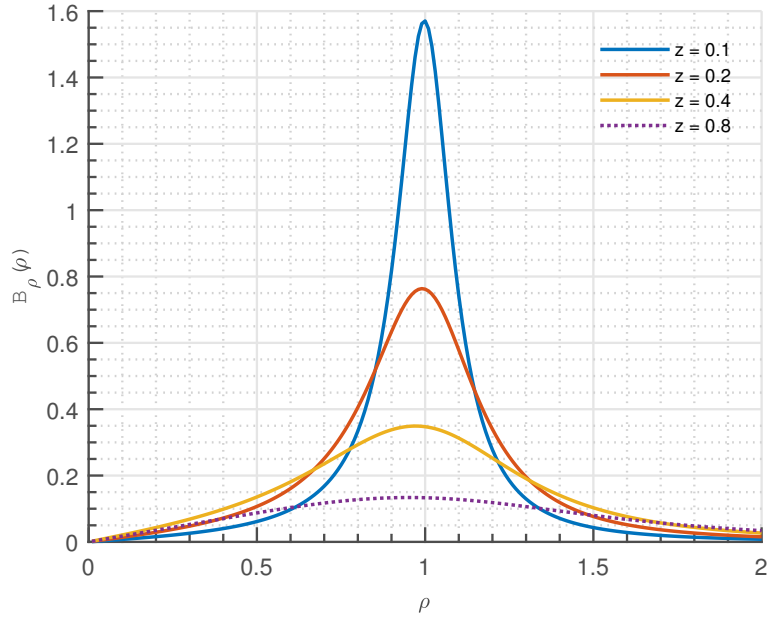

Figure 3.4: Radial magnetic field as a function of distance from the symmetry axis for 4 distances along the axis: $z = 0.1a, 0.2a, 0.4a$ and $0.8a$

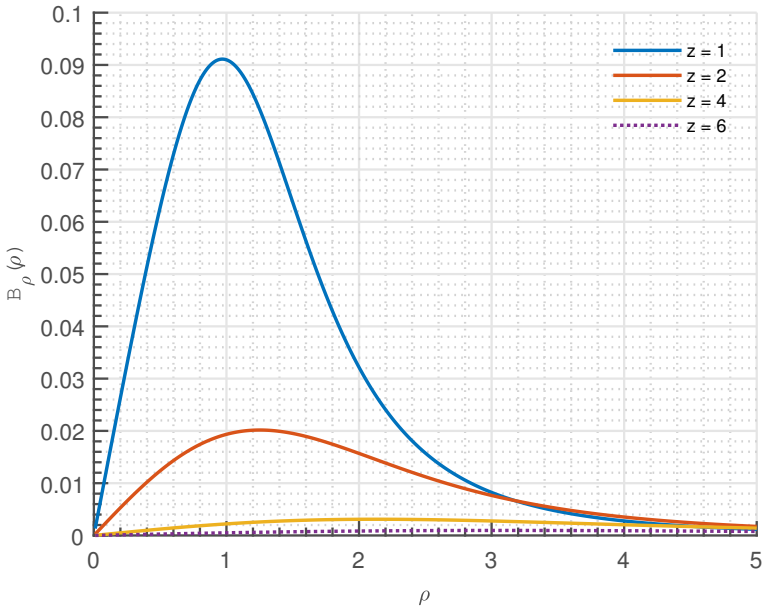

Figure 3.5: Radial magnetic field as a function of distance from the symmetry axis for 4 distances along the axis: $z = a, 2a, 4a$ and $6a$

3.3 Mutual Inductance between two circular loops

We will in this section calculate the mutual inductance between two circular loops.

Coaxial loops We consider the mutual inductance between two coaxial circular loops. The first loop, loop 1, has radius a and is located in the xy plane, centered at origin. The second loop, with a radius b is located in a plane parallel to and a distance z away from the xy plane. We are interested in the mutual inductance between the two loops caused by a current I in the first loop. It is shown in appendix that the mutual inductance for two coaxial circular loops is

$$M = \frac{2\mu_0 ab}{\sqrt{(a+b)^2+z^2}} \frac{(2-m^2)K(m) - 2E(m)}{m^2} \tag{3.21}$$

, where

$$\alpha^2 = (a-b)^2 + z^2 \tag{3.22}$$

$$\beta^2 = (a+b)^2 + z^2 \tag{3.23}$$

$$m^2 = 1 - \frac{\alpha^2}{\beta^2} \tag{3.24}$$

It is sometimes useful to have a simplified expression for the mutual inductance avoiding the two complete elliptic integrals. However, it is shown in appendix A that replacing the elliptic integrals with their Taylor series form gives an expression that is useful only in the farfield. By manipulating the expressions for the elliptic integrals, we have shown that a more useful approximation for the mutual inductance is to the first order:

$$M_1 = \frac{4\pi\mu_0 (ab)^2}{(\beta+\alpha)^3} \tag{3.25}$$

The first and second order approximation are shown in figure 3.6 and the relative error using the approximations are shown in figure 3.7.It is seen that the even the first order approximation is valid for separation of one radius and above.

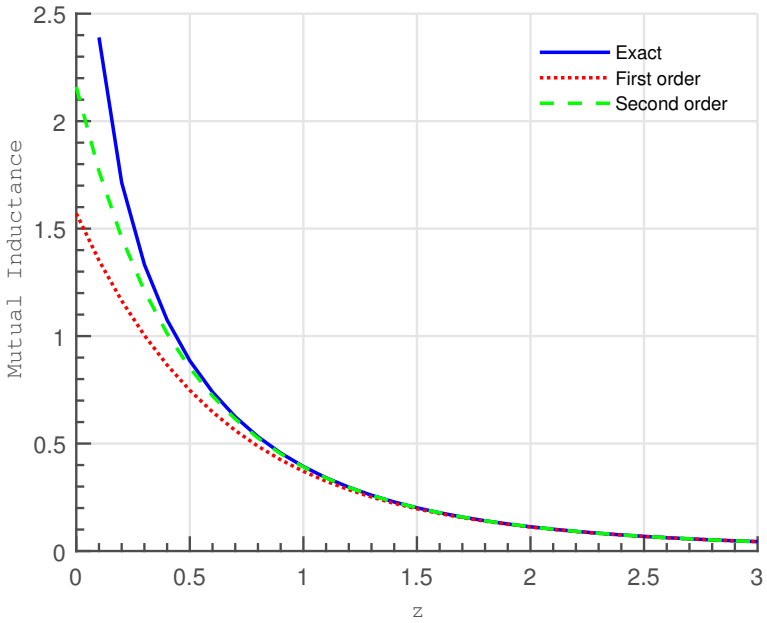

Figure 3.6: Mutual inductance between two coaxial, equal sized coils as a function of separation. The first (non-vanishing) and second order new approximations are included.

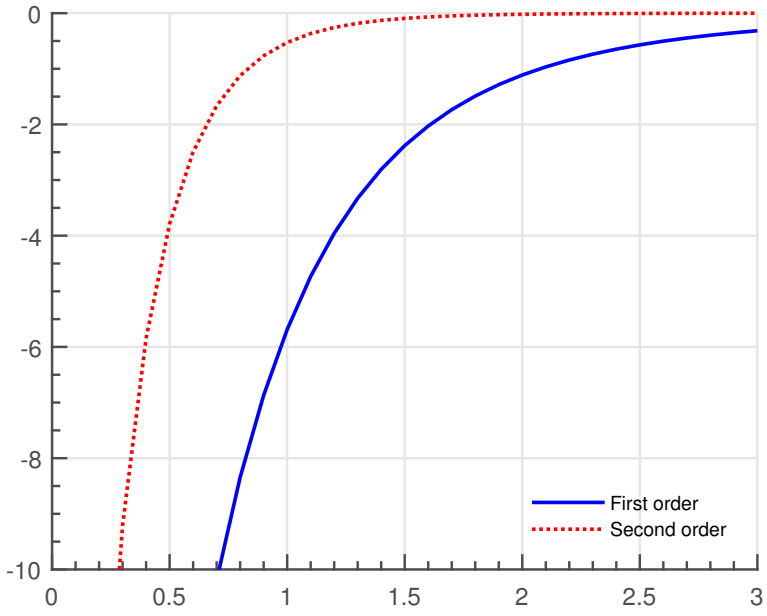

Figure 3.7: Relative error by using the new first and the second order approximation for the mutual inductance between two coaxial, equal sized coils as a function of separation

3.3.1 Lateral displaced loops

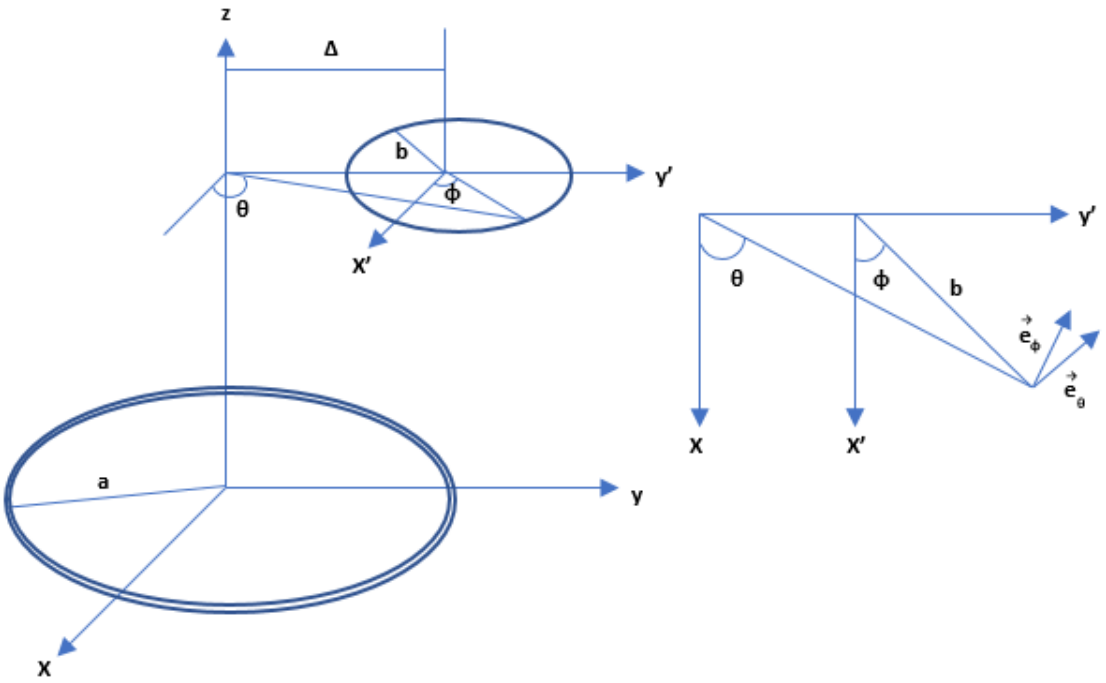

Figure 3.8: Coil with lateral displacement. The receiving coil is displaced a distance Δ form the axis at a distance Z from the transmitting coil. To the right is a projection of the geometry to the xy plane.

Again we consider two circular coils, the transmitter with radius a and center in origo, and the receiver with radius b in a plane parallel to the xy-plane. The receiver is an axial distance z from the transmitter and is displaced laterally a distance Δ. The configuration is shown in 3.8. In Appendix A, it is shown that for this configuration the mutual inductance may be expressed as:

$$M = \frac{2\mu_0 ab}{\pi} \int_0^\pi d\phi \frac{b + \Delta \cos\phi}{\rho\beta} \Gamma(m) \tag{3.26}$$

Here we have:

$$\alpha^2 = (a - \rho)^2 + z^2) \tag{3.27}$$

$$\beta^2 = (a + \rho)^2 + z^2) \tag{3.28}$$

$$\Gamma(m) = \frac{(2 - m^2)K(m) - 2E(m)}{m^2} \tag{3.29}$$

$$m^2 = 1 - \frac{\alpha^2}{\beta^2} \tag{3.30}$$

It has not so far been possible to find an exact analytic expression for M from eq. 3.26 and it had to be integrated numerically. The mutual inductance as a function of lateral displacement has been calculated for several distances from the transmitter. The results are shown in figures 3.9 and 3.10. The effect of the large variation of the magnetic field close to the wire is apparent even in the mutual inductance.

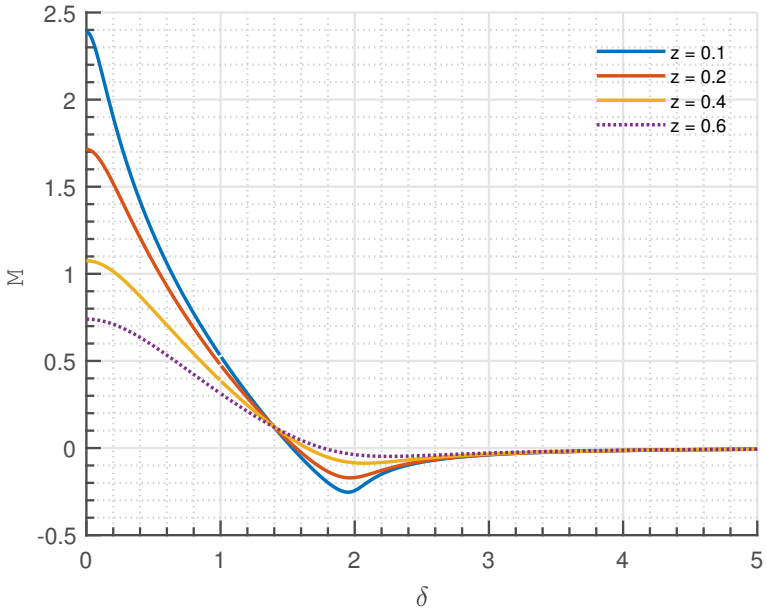

Figure 3.9: Mutual inductance between two coaxial, equal sized coils as a function of lateral separation for axial distances $z = 0.1a, 0.2a, 0.4a, 0.6a$

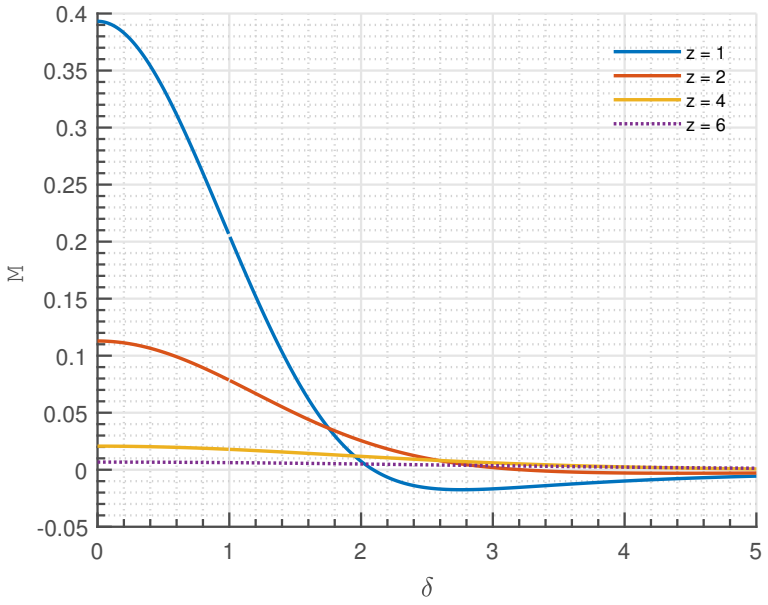

Figure 3.10: Mutual inductance between two coaxial, equal sized coils as a function of lateral separation for axial distances $z = a, 2a, 4a, 6a$

3.3.2 Summary

The most important relationship required for position control in IPT is how the coupling coefficient or mutual inductance varies with position. We have modelled the magnetic field from a thin circular wire for this purpose.

The magnetic field from a circular loop can be expressed in closed form as a weighted sum of elliptic integrals and has been known for years. The magnetic field has here been calculated and implemented, in Matlab, for two reasons; One is that the magnetic field gives and indication of the possible variations in the mutual inductance. The other reason is that it can be used to verify the calculation of the magnetic flux and thus the mutual inductance.

The mutual inductance between two circular coils is much more complicated to calculate than the magnetic field, and only the case with coaxial loops is known in closed form. One result in this chapter is that we have developed an approximate expressions that is valid for small distances between the two coils. A model has been developed for two special cases: for relative coaxial movement along the axis of symmetry and relative movement of the receiver in a plane parallel to the transmitter plane. In the model, the two coils don't need to be equal size.

Chapter 4

Frequency response for IPT systems

One of the main objective of this work has been to investigate how position control compares with state-of-the-art methods for inductive power transfer control.In order to do a qualitatively and quantitatively comparison, we need to be able to calculate the result from state-of-the-art methods. What is considered state-of-the-art depends on the application, (11), but for inductive power transfer for high power, high efficiency systems the recent work of Giuseppe Guidi and Jon Are Suul, both (17) and (18) and pending patents, would definitely count as state-of-the art.

In this chapter the frequency characteristics for an SS compensated inductive power transfer (IPT) system are described and give some specific examples. The discussion given here is based on Guidi (17) and Guidi and Suul (18), who has derived the transfer function for the lossless case. They also discusses the case with loss, but does not provide the transfer functions for it. In Appendix B several transfer functions for SS compensated is derived for a lossy case. The lossless case will of course only be a special, simplified case. Only the results and some examples are given here.

The transfer functions for a SS-compensated IPT configuration will be of great importance when designing and tuning the system. Some of the transfer functions will the basis for the simulation model, and will be discussed in greater detail in Chapter 5.

4.1 Introduction

All IPT systems operating in resonant mode requires tuned circuitry in both receiver and sending circuits in order to achieve high throughput with minimum losses. One form of compensation, is SS compensation which means that both sending and receiving circuits has series compensation. SS compensated IPT system was the main focus of Guidi and Sul and this is the case that will be discussed here. For the other three combination of series and paralell compensation, the reader is referred to Wang et al. (29). It will be relatively easy to extend the work done here to the other forms of compensation circuitry.

Figure 4.1 shows a simplified topology for an IPT circuit with SS compensation. Most of the symbols used are standard, with M being the mutual inductance between the two circuits. A cautious note about notation is in place here: In this thesis, we have chosen to use p and s as subscripts for the primary (sending) and secondary (pickup) circuit, respectively. This is the convention that is most common in literature. It should be noted however, that in in some of the papers cited, p and s is used as subscript for pickup and sending circuits, respectively, which may sometimes be a bit confusing. In deriving the frequency characteristics we have used Laplace transform, and use $s = j\omega$ to convert the result to frequency.

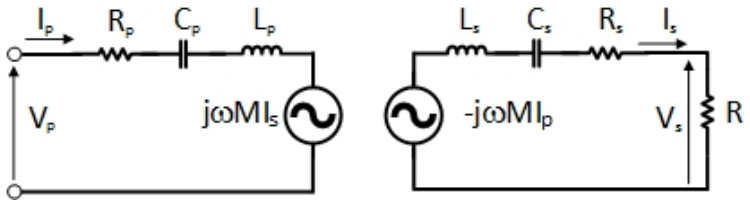

Figure 4.1: Circuit topology for series compensated primary and secondary circuit

The transfer functions has been derived for two cases:

- Constant Resistive load (CRL)
- Constant voltage load (CVL)

4.2 Transfer functions

The most useful transfer functions and relations are listed here. The **transfer function from primary current to secondary current** is:

$$G_{i,ss} = \frac{i_s}{i_p} = \frac{M\omega_s s}{Z_s + \frac{2\zeta}{\omega_s C_s}} \tag{4.1}$$

The **sending impedance** is the impedance seen from the input terminals:

$$Z_{pt} = \frac{v_p}{i_p} = Z_p - \frac{M^2\omega_s^2 s^2}{Z_s + \frac{2\zeta}{\omega_s C_s}} \tag{4.2}$$

The sending impedance may be expressed as

$$Z_{pt} = Z_p + Z_r \tag{4.3}$$

, where Z_r is the **reflected impedance**:

$$Z_r = -\frac{M^2\omega_s^2 s^2}{Z_s + \frac{2\zeta}{\omega_s C_s}} \tag{4.4}$$

The reflected impedance may be thought of as the impedance of the secondary circuit as seen from the primary circuit. The last transfer function is the **transfer function from primary voltage to secondary voltage**:

$$G_{v,ss} = \frac{v_s}{v_p} = \frac{R}{Z_{pt}} G_{i,ss} \tag{4.5}$$

The **complex power transferred to the load** is

$$S_l = v_s i_s^* = \frac{G_{v,ss} G_{v,ss}^*}{R} |v_p|^2 \tag{4.6}$$

The **complex power transferred to the secondary circuit** is

$$S_p = v_r i_p^* = \frac{Z_r}{Z_{pt} Z_{pt}^*} |v_p|^2 \tag{4.7}$$

The **power transferred to the secondary circuit** is thus

$$P_p = Re(Z_r) \frac{|v_p|^2}{|Z_{pt}|^2} \tag{4.8}$$

Primary	Secondary
Parameters:	
$C_p = 42.2\,\text{nF}$	$C_s = 42.2\,\text{nF}$
$L_p = 32.7\,\mu\text{H}$	$L_s = 32.7\,\mu\text{H}$
$Q_p = 150$	$Q_s = 150$
$k = 0.35$	
Calculated:	
$R = 9.743\,\Omega$	
$f_p = 135\,\text{kHz}$	$f_s = 135\,\text{kHz}$

Table 4.1: Parameters used for case with loss

4.2.1 Resistive Load

We will here give some examples of the transfer functions given in the last section for constant resistive load. We consider two cases. The first example is with loss and the parameters are given in table 4.1. The other example is without loss, which is the same except that $R_p = R_s = 0$ ($Q_p = Q_s = \infty$). The current-to-current transfer function for the case of purely resistive load is:

$$G_{i,ss} = \frac{i_s}{i_p} = \frac{M\omega_s^2 C_s s^2}{s^2 + 2(\zeta_s + \zeta)s + 1}$$

Figure 4.2 shows the secondary to primary current transfer function for the parameters in table 4.1. As long as the secondary circuit resistance is a lot smaller than that of the load resistance it will not alter the transfer function. Thus the lossless case is more or less identical to that in figure 4.2.
The reflected impedance is:

$$Z_r = -\frac{M^2\omega_s^3 C_s s^3}{s^2 + 2(\zeta_s + \zeta)s + 1} \tag{4.9}$$

Figure 4.3 shows the reflected impedance for the lossless case. The case with $Q_p = Q_s = 150$ is almost identical to the lossless case, so $Q_p = Q_s = 15$ is shown for comparison with the lossless case. The expression for the sending impedance, eq. 4.3, is a bit more complicated than the two previous expressions:

$$Z_{pt} = \frac{\eta^2(1-k^2)s^4 + 2\eta[\zeta_p + \eta\zeta_T]s^3 + [\eta^2 + 1 + 4\zeta_p\zeta_T]s^2 + 2[\eta\zeta_p + \zeta_T]s + 1}{s\omega_s C_p[s^2 + 2\zeta_T s + 1]} \tag{4.10}$$

With $G_{i,ss}$ and Z_pt known, the transfer function from primary to secondary voltage may be calculated from 4.5. This transfer function is shown in Figure 4.4

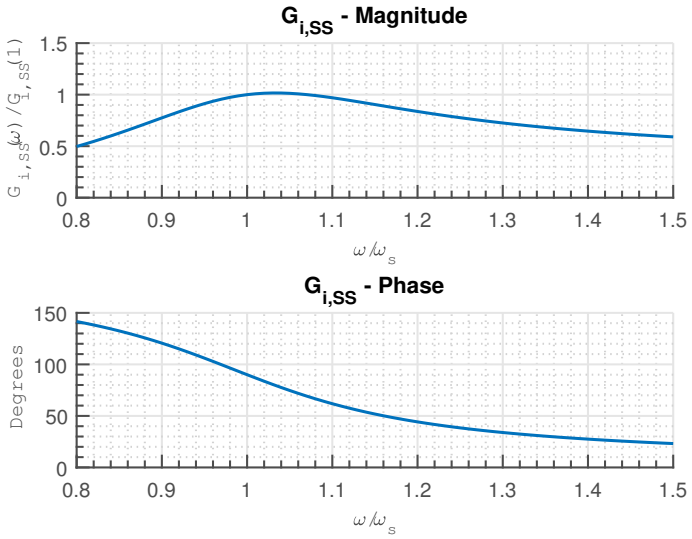

Figure 4.2: CR - Secondary to primary current transfer function for $k = 0.35, Q_p = Q_s = 150$

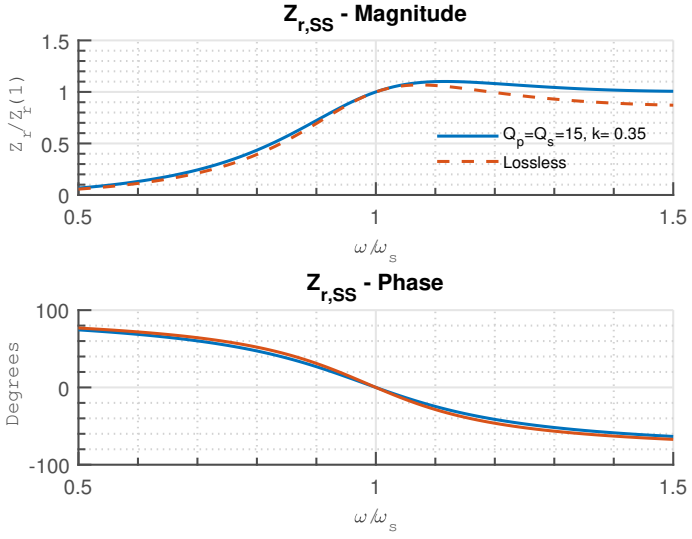

Figure 4.3: CR- Reflected impedance for $k = 0.35, Q_p = Q_s = 15$ and lossless

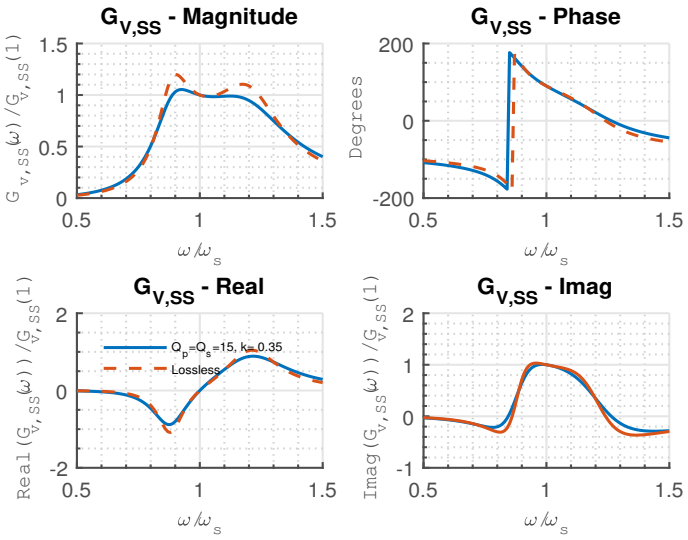

Figure 4.4: Primary to secondary voltage transfer function for $k = 0.35, Q_p = Q_s = 15$ and lossless

Lossless case We now consider the lossless case, $\zeta_p = \zeta_s = 0$, with equal primary and secondary circuit resonance frequencies, $\eta = 1$. In this case, the sending impedance is:

$$Z_{pt} = \frac{2\zeta k^2\omega^5 - j(1-\omega^2)[(1-\omega^2)^2 - k^2\omega^4 + 4\zeta^2\omega^2]}{\omega\omega_s C_p[(1-\omega^2)^2 + 4\zeta^2\omega^2]} \tag{4.11}$$

From this result it is clear that the reactive part of the sending impedance is zero for $\omega = 1$ as expected. However, there may potentially be four more zeros for the reactive part of the sending impedance. These possible zeros is the solution of the equation:

$$(1-\omega^2)^2 - k^2\omega^4 + 4\zeta^2\omega^2 = 0 \tag{4.12}$$

For an ideally matched load, this equation has real solutions only if

$$k \geq k_0\sqrt{1 - \frac{k_0^2}{4}} \tag{4.13}$$

This means that in order to avoid bifurcation, the requirement for the operation of a lossless IPT system is

$$k < k_0\sqrt{1 - \frac{k_0^2}{4}} \tag{4.14}$$

4.2.2 Constant Voltage Load

We will now consider a system in which the load voltage is constant. The load can not be modelled as an equivalent constant resistance, and although the functional relationship between output current and output voltage can be modelled as

$$v_s = Ri_s \tag{4.15}$$

R will now depend both on frequency and also on the load voltage. The phase of the secondary current must be equal to the phase of the secondary voltage, which means that R will be real. We see that if the angle between the current and voltage is zero(in phase), the load is purely real and only active effect is dissipated. It is possible to find an explicit expression for R as a function of supply and load voltages. However, here we will only give the implicit expression for R;

$$\begin{aligned} -[M^2\omega_s^2 s^2\frac{|v_p|^2}{|v_s|^2} + |Z_p|^2]R^2 &= |Z_pZ_s - M^2\omega_s^2 s^2|^2 \\ &+ 2R[|Z_p|^2 R_s - M^2\omega_s^2 s^2 R_p] \end{aligned} \tag{4.16}$$

We will here give some examples of the transfer functions for the constant voltage load. We consider two cases. The first one is given in table 4.2. The other example is without loss, $R_p = R_s = 0$ ($Q_p = Q_s = \infty$). Figure 4.5

Primary	Secondary
Parameters:	
$C_p = 42.2\,\text{nF}$	$C_s = 42.2\,\text{nF}$
$L_p = 32.7\,\mu\text{H}$	$L_s = 32.7\,\mu\text{H}$
$Q_p = 150$	$Q_s = 150$
$k = 0.35$	
Calculated:	
R =9.743 Ω	
$f_p = 135\,\text{kHz}$	$f_s = 135\,\text{kHz}$

Table 4.2: Parameters used for case with loss

shows the load resistance for the lossless case and for $Q_p = Q_s = 150$.

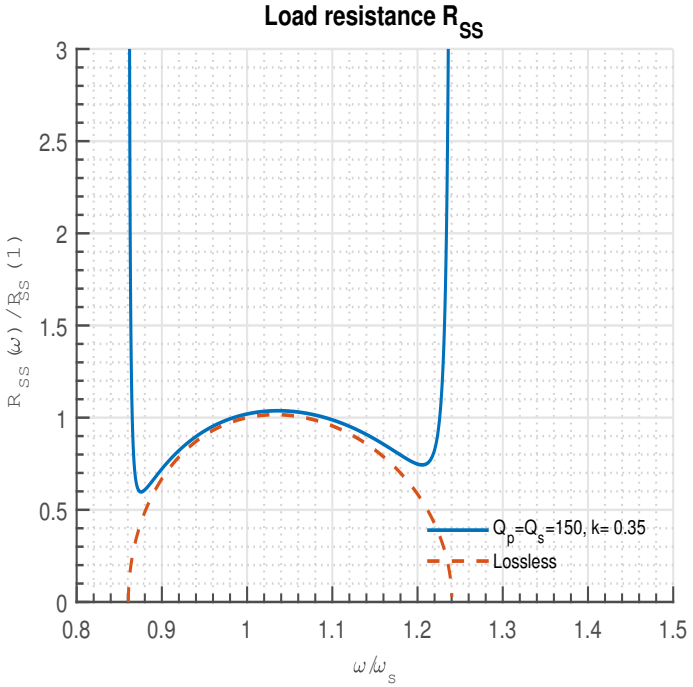

Figure 4.5: CV - Load Resistance for $k = 0.35, Q_p = Q_s = 150$ and lossless

Figure 4.6 shows the power transferred to the load for the lossless case and for $Q_p = Q_s = 150$.

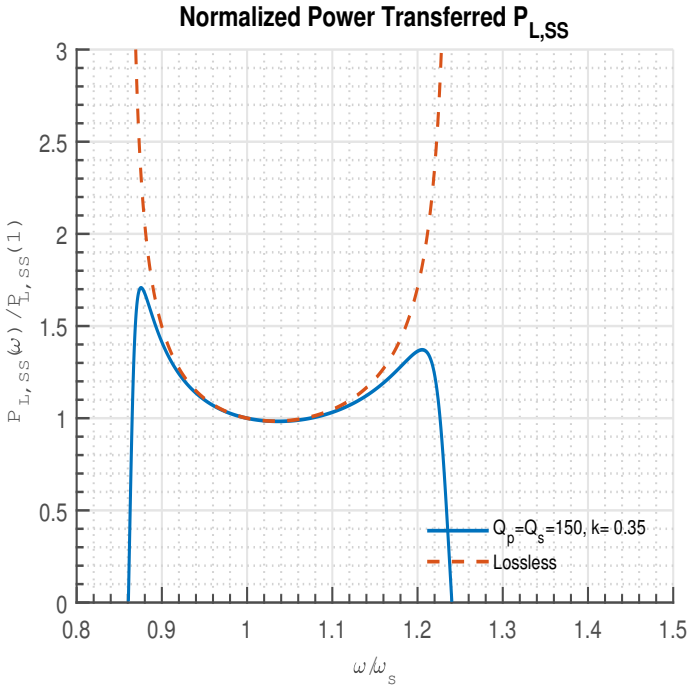

Figure 4.6: CV- Power transferred for $k = 0.35, Q_p = Q_s = 150$ and lossless

Figure 4.7 shows the sending impedance for the lossless case and for $Q_p = Q_s = 150$.

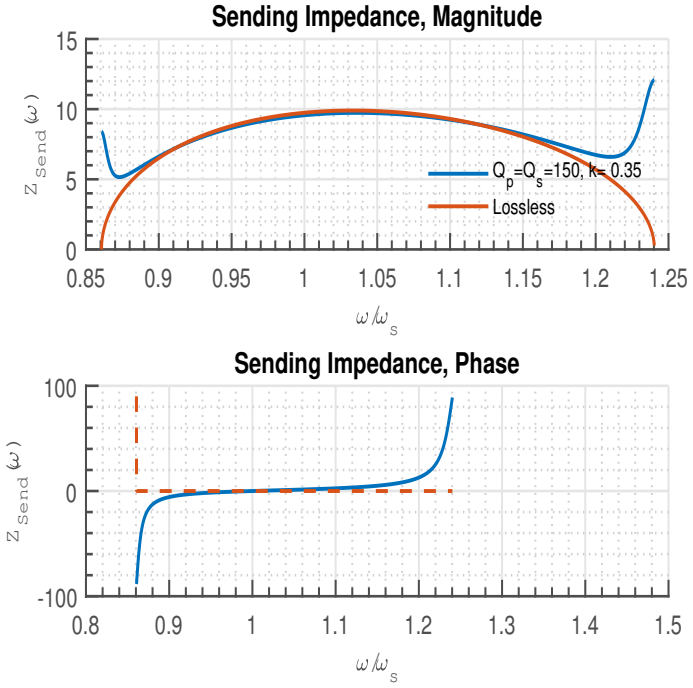

Figure 4.7: Sending impedance for CV for $k = 0.35, Q_p = Q_s = 150$ and lossless

Lossless case For the lossless case, $R_s = R_p = 0$, the equation for the load resistance simplifies a lot and it is shown in Appendix B that:

$$R = \frac{1}{\omega_s C_s |s|} \frac{|\eta^2(1-k^2)s^4 + (\eta^2+1)s^2 + 1)|}{[\eta^4(\frac{k^2}{x_\mu^2} - 1)s^4 - 2\eta^2 s^2 - 1]^{\frac{1}{2}}} \tag{4.17}$$

Since R has to be real, the expression under the root sign has to be nonnegative. With $s = j\omega$ this requires that

$$\left[1 - \eta^2(1 - \frac{k}{x_\mu})\omega^2\right]\left[(1 + \frac{k}{x_\mu})\eta^2\omega^2 - 1\right] > 0 \tag{4.18}$$

and

$$\frac{\omega_p}{\sqrt{1+\frac{k}{x_\mu}}} < \omega < \frac{\omega_p}{\sqrt{1-\frac{k}{x_\mu}}} \tag{4.19}$$

, which is the range for which operation is possible in the constant voltage case

In figure 4.8 we see a comparison between a SS-IPT system with optimally matched CR load at resonant frequency, and a system with CV load.

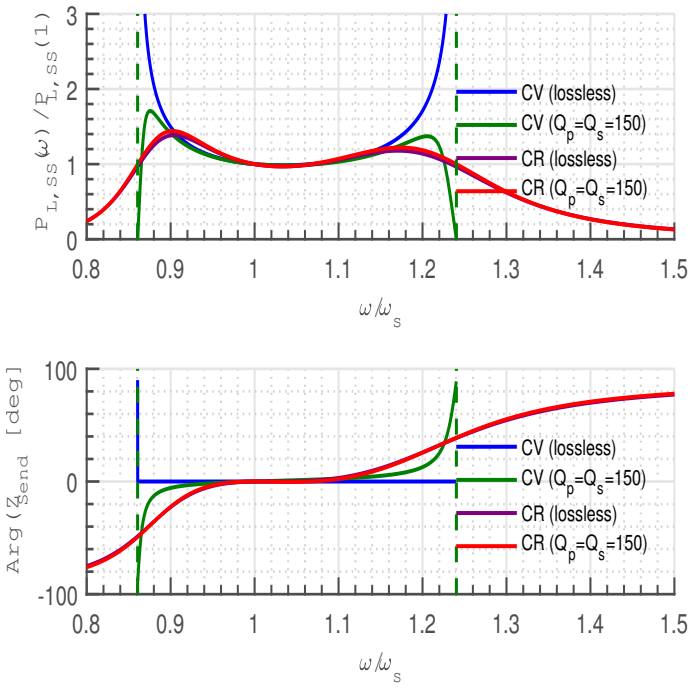

Figure 4.8: CR load CV load

4.3 Summary

The mathematical expressions for the various transfer functions for an SS-compensated IPT system from the basic circuit equations have been derived. These expressions have been implemented in Matlab, and we are now able to calculate transfer functions and power output for any SS compensated IPT system with CR or CV load. The transfer functions for the lossless case has been verified by comparing our results with the result from (18). Without access to the expression for the transfer functions for the lossy case, the results have been verified by comparing plots of transfer functions with corresponding ones in the aforementioned paper. One example is 4.8 and figure 5 in (18).

Chapter 5

Results

In this chapter we will present the design of the IPT system used in the simulation, as well as the parametric values of the individual components. The position controller will be explained, and we will show how they all come together in the simulink model. For the simulations themselves, we will be looking at two different cases of misalignment; axial and lateral. Within each case we will look at the system response for a few different types of input, to get a better understanding of the behaviour of the system given different operating conditions.

For the two cases of axial and lateral misalignment, an attempt to explain the relationship between the offset distance and the coupling coefficient will be provided. I would however like to preface that the relationship between the two are quite complex, and beyond the scope of a master thesis.

Before the model and results for the two cases are given, we revisit the control theory which is applicable to add some context:

Regulation and Tracking Suppose the reference signal to a state feedback system is zero and the response of the system is caused by some nonzero initial conditions. The problem is to find a state feedback gain so that the responses in the system will die out at a desired rate. This problem is referenced to as the *regulator problem*. This setting can be seen in many aspects of industry: maintaining liquid levels in a tank, and maintaining a steady course through use of auto pilot. A related problem is that of tracking. Suppose that the reference signal is constant. Then the problem is to design a system so that the output converges to the reference signal when time move

towards infinity. This is called *asymptotic tracking* of a step reference input. If the reference signal is not constant, the tracking problem of the signal is called *servomechanism problem*(9). It is a problem of this nature that is examined in this section; how to track the ship as it is subjected to waves to ensure the most effective power transfer.

Position Control How to position a flexible mechanical armature to follow a ship being subjected to waves, while ensuring the most effective power transfer is the problem being explored. One must determine the voltage input to the motor controlling the movement and speed of the armature, such that it tracks the motion of a ships hull. The combination of the distance sensor, regulator and the armature has to be exceedingly faster than the wave dynamics, as a minor change in the k-factor results in a significant loss of effectiveness 2.10. A fast position control regulator can be obtain through pole placement manipulation; a procedure to place the closed-loop poles of the plant in predetermined locations in the s-plane.

5.1 IPT model

The IPT is designed such that it delivers P_{rated} to the load, at a fixed frequency ω_0, and a high quality factor. Using the model, it will be shown how an offset from the nominal distance affects the coupling coefficient, and as a consequence the output power through the relationship given in equation 2.10. The loss in output power is compensated by increasing the primary current to maintain rated power delivered to the load. The drawback is a that an increase in the primary current also will of lower the overall efficiency of the circuit. Even so, the decision here is to focus on keeping the coupling variations as low as possible, as it allows for the use of a lower rated converter, as described by equation 2.11.

Table 5.1 shows the values used in the setup. The theoretical efficiency is calculated from equation 2.9. Coil material and shape have not been considered, and we are therefore assuming no magnetic losses. r_p and r_s are the radius of the primary and secondary coil, respectively. D_{nom} is the nominal axial distance used in all the simulations.

Table 5.1: IPT Metrics

P_{Rated}	10	kW
ω_0	15	kHz
L_p	300	mH
L_s	300	mH
C_p	14.82	nF
C_s	14.82	nF
k_{nom}	0.59	
Q_S	150	
D_{nom}	0.10	m
r_p	0.20	m
r_s	0.20	m
η	98.32	%

5.1.1 Position Control

As mentioned earlier, in order to have a fast, precise and stable position controller, so that the plant output follows the reference as close as possible, a detailed physical description of the system, or mathematical equations for modeling the system, are needed. In this thesis we are not looking at a specific system and will model the control as a servomechanism. This controller uses error sensing negative feedback to reduce or eliminate the error. The input to the controller is the positional difference between the secondary coil current position, and it's nominal position. Below is a schematic of the controller:

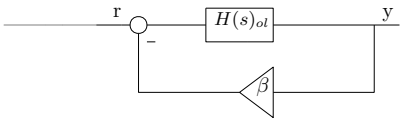

Figure 5.1: Negative Feedback Controller

The controller then act as a self-controlling process, and can be thought of as the physical system responsible for moving the primary coil and the regulator, represented as one. The controller is designed to have a phase displacement, to represent the imagined inertia of the physical system.
$H(s)_{ol}$ is the open loop transfer function, and β is the feedback factor, that governs the amount fed back from the output signal. Together they form the closed loop transfer function that describes the controller $H(s)_{cl}$. The following values where used:

$$H(s)_{cl} = \frac{83.33}{s^2 + 22.83s + 83.33} \tag{5.1}$$

With its gain and frequency characteristics given in C.1.

5.2 System model

The complete system model is shown in figure 5.2 with the source feeding the regulator the measured offset(m) from the set point value. The regulator then attempts bring the offset back to zero again. The result is then sent to a block that generates a coupling coefficient based on nominal operating distance and the remaining position error supplied by the regulator. The formula is different for the two cases of axial and lateral offset. The coupling coefficient is then fed to the IPT system which calculates power output according to equation 2.10.

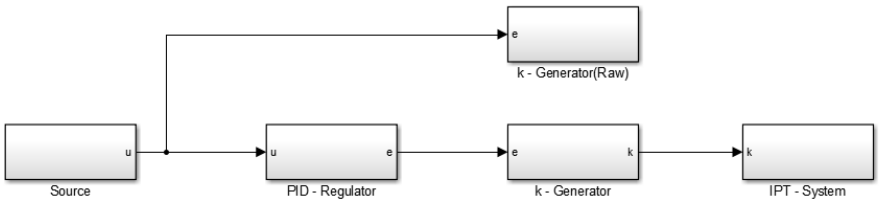

Figure 5.2: System Model

5.3 Use cases

We will look at three different scenarios

- Step Response - A sudden change in position
- Wave Dynamics - A slowly varying position
- Drift - A shift to a new position

The **impulse response** shows how the controller handles a sudden shift in distance. The desired response of the controller is to reach the desired value, in this case zero offset between the primary and secondary coil, as fast as possible, with little to no oscillations before settling, to minimize the amount of movement.

The **wave response** subjects the system to a continuous sine wave, where the amplitude is the distance we will drift across our optimal point. In the case of axial displacement this signal is bounded due to the potential collision between primary and secondary coils at higher amplitudes. There are no bounds on the movement in the opposite direction.

Noise is added to the wave signal, in order to see what effects it will have on the system and make the scenario more realistic, as the input in most real applications rarely consists of a pure sine wave with no harmonics.

Unlike the instantaneous movement of the impulse response, the **drift response** is a ramp function that mimics a movement from the nominal operating point to a new point a set distance away, with a given parameter for the speed of the change in position. The set distance used equates to a change in coupling coefficient of 275% to use as a basis for comparison against the results of (18).

5.4 Axial Displacement

Introduction

Axial displacement is a relative movement of the secondary coil along the common central axis of the two coils, either towards (negative movement) or away (positive movement) from the primary coil. In this case it is considered to be the only degree of freedom the system will exhibit during the simulation.The concept is illustrated in fig 5.3 below.

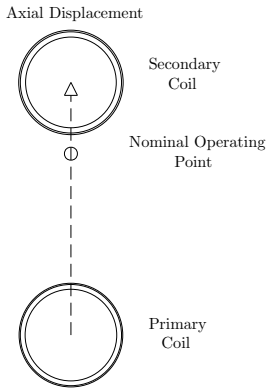

Figure 5.3: Axial - Displacement

Coupling Coefficient

The coupling coefficient for the Axial case is modeled after equation A.35 with the use of equation 2.5 to get the coupling coefficient.

Parameters

Below is a list of key parameters used in the simulations.

- Step Response - Step value of 0.1 at 10 seconds
- Wave Dynamics - Amplitude of 0.05 at a frequency of 0.125 Hz
- Ramp Response - Slope of 0.0042 equals a variance in k of 275%

5.4.1 Simulations

Step Response

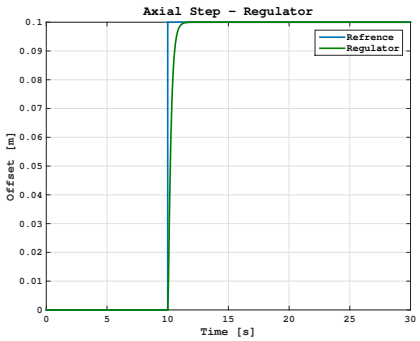

Figure 5.4: Step Response

In figure 5.4 we see a step of 0.1 metres away from the secondary coil. This is a doubling in value from the nominal operating point. As can be see the system is quick to catch up, taking about 2 seconds before nominal operating value is regained.

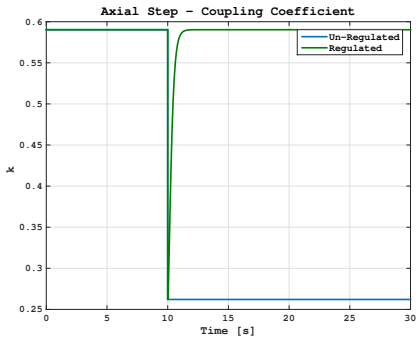

Figure 5.5: Step Response - Coupling Coefficient

As suspected we see from figure 5.5 that the coupling coefficient plummets, experiencing a 227 % change. We see the massive impact this has on the output power in figure 5.6 where a doubling from that of the nominal operating distance, reduces the output power to one fifth of the rated value.

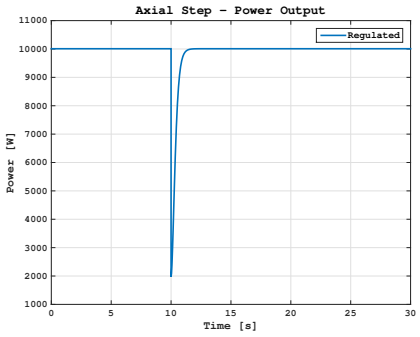

Figure 5.6: Step Response - Output Power

Slow Moving Waves

From figure 5.7 it can be seen that we are lagging a little behind the reference value, as was wanted. The delay is caused due to the error passed on through the system is also a sine wave with an amplitude of about 0.01 m. This means we have a variation of 20% (11cm - 9cm) around the nominal set point(10 cm). We see how this affects the coupling coefficient in figure 5.8. The change in coupling is about 18% from k_{min} to k_{max}, which is in stark contrast to the case of no position control, where the change is over 250%. We also see that the effects of the noise is beginning to become noticeable.

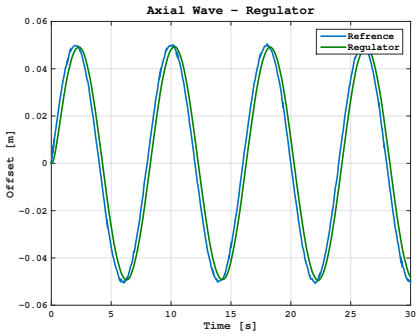

Figure 5.7: Wave Dynamics

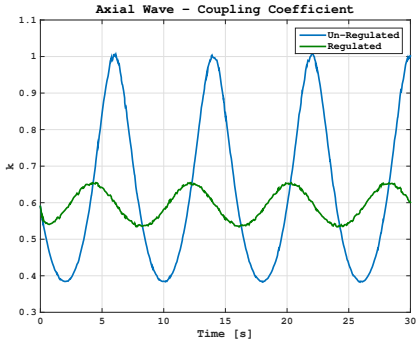

Figure 5.8: Wave Dynamics - Coupling Coefficient

Now the noise is quite prevalent in 5.9. Also take note of the variation in power delivered to the load is about 50 %; because we do not stray too far from the nominal operating point, the impact on the output power is not that severe.

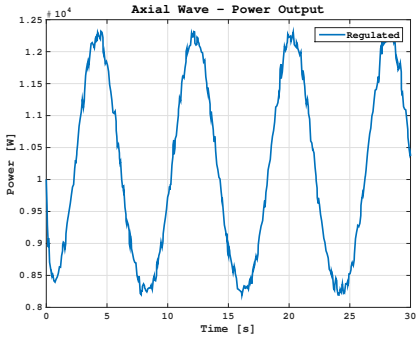

Figure 5.9: Wave Dynamics - Output Power

Drift

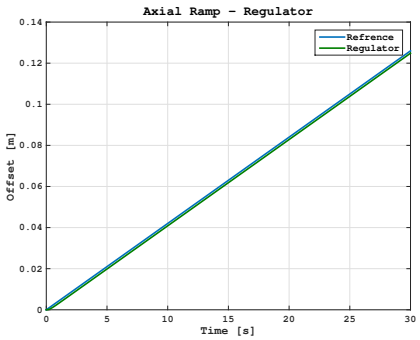

Figure 5.10: Ramp Response

In figure 5.10 we see the secondary coil is slowly drifting away from the primary coil, though as seen the regulator keeps the primary coil in tow. The movement of a little over 12 cm equates to a 275% change in coupling coefficient as seen in figure 5.11.

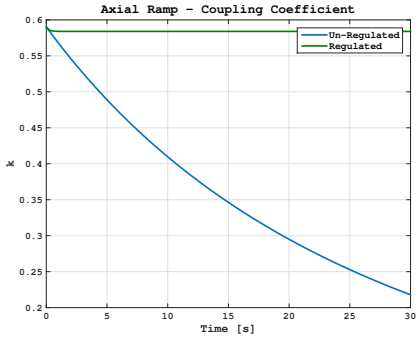

Figure 5.11: Ramp Response - Coupling Coefficient

Note the slight difference from the reference value in 5.11, is due to the feedback controller having a small error, as its gain is not a perfect 1. This small error is then up scaled trough out the process and end up as a 2% error in the output power, seen in figure 5.12.

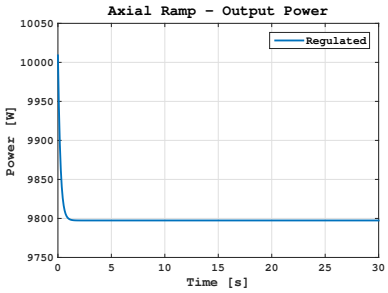

Figure 5.12: Ramp Response - Output Power

5.5 Lateral Displacement

Introduction

Lateral displacement is the movement of the secondary coil parallel to the primary coil in x or y direction, with z direction being the axial movement. In this case we only consider movement in the x direction for the simulations. The movement is equal to that of y direction, as the coils are thought of as perfectly circular. Movement is illustrated in fig5.3 below

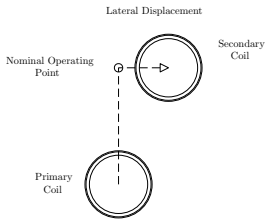

Figure 5.13: Lateral - Displacement

Coupling Coefficient

The coupling coefficient for the Lateral case is modeled after equation A.51 with the use of equation 2.5 to get the coupling coefficient.

Parameters

Below is a list of key parameters used in the simulations.

- Step Response - Step value of 0.4 at 10 seconds
- Wave Dynamics - Amplitude of 0.4 at a frequency of 0.125 Hz
- Ramp Response - Slope of 0.007 equals a variance in k of 275%

5.5.1 Simulations

Step Response

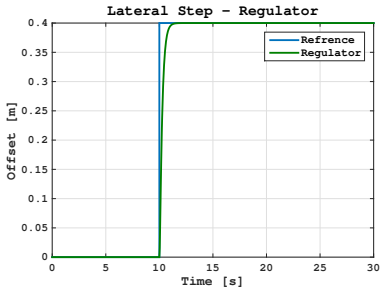

Figure 5.14: Step Response

From figure 5.14 we see the regulator follows the reference at a reasonable rate, which was to be expected as the only thing that has changed from the axial case is the step value, from 0.1 axial displacement to 0.4 lateral displacement. This distinction is not something the controller is concerned with, as it only task is to drive the perceived offset to zero.

There is, however, a noticeable difference when we look at figure 5.15, where the coupling coefficient drops below zero. Remember the coupling coefficient is defined as $k \in [0, 1]$; the reason it turns negative here is because the mutual inductance becomes negative, and the way the coupling coefficient is calculated in the model, it does not correct for such an occurrence. The radius of both coils are as mentioned earlier 20 cm, and a displacement of 40 cm will have the primary and secondary coils side by side seen from the lateral plane. Despite the nominal axial distance separating them is still 10 cm, the mutual inductance goes negative because opposing magnetic field supersedes the original magnetic field.

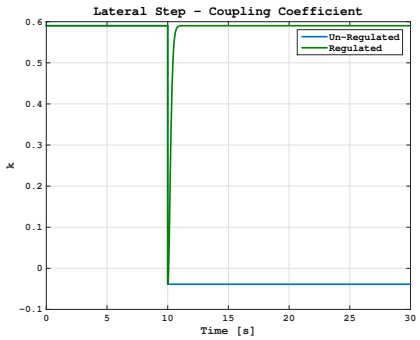

Figure 5.15: Step Response - Coupling Coefficient

As to be expected there is no power transferred for an instance as can be seen in figure 5.16.

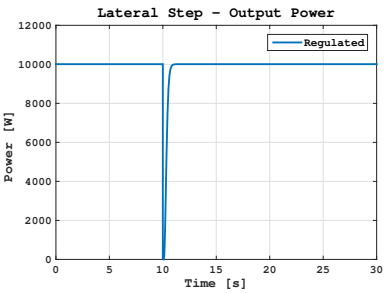

Figure 5.16: Step Response - Out Power

Slow Moving Waves

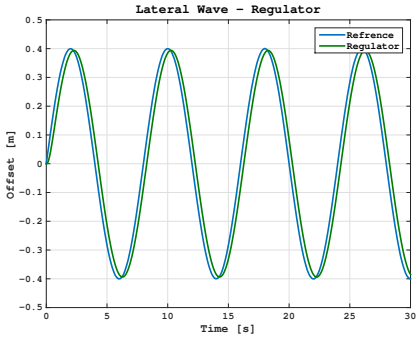

Figure 5.17: Wave Dynamics

Again we see the regulator lagging a little behind 5.17, which is the same as for the axial case. There are however prominent differences when looking

at the coupling coefficient in figure 5.18, where we can see the unregulated case really suffers from spending such a long time in the area where the mutual inductance plummets. This is not the case with the regulated case, where the coupling coefficient varies by approximately 20 % , which is about the same as for the axial case. Notice however that the axial case also had 20% movement variation, while the lateral case has 42.5% variation, with a variation amplitude of 8.5 cm.

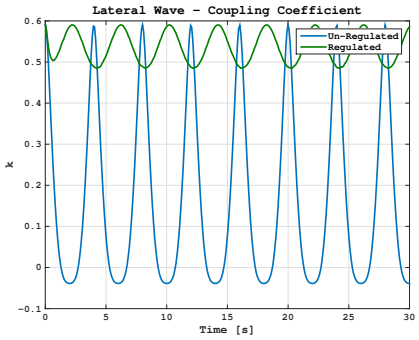

Figure 5.18: Wave Dynamics - Coupling Coefficient

In figure 5.19 we can see we have a 43% variation in output power, and that the variation is not around the rated output power of 10000 kW, but have dropped to 8500 kW.

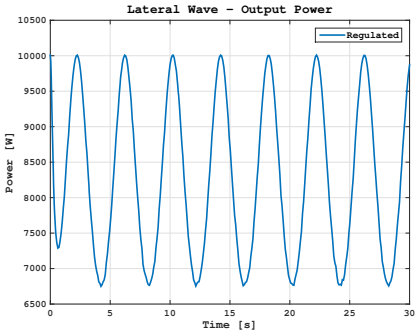

Figure 5.19: Wave Dynamics - Out Power

Drift Response

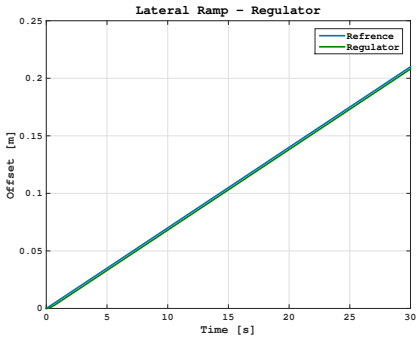

Figure 5.20: Simulation: Drift Response

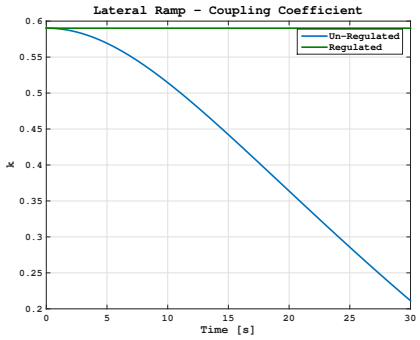

Figure 5.21: Simulation: Drift Response - Coupling Coefficient

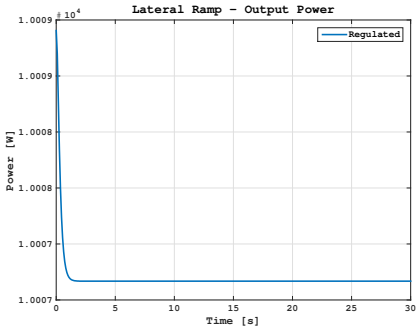

Figure 5.22: Simulation: Drift Response - Output Power

We can see that the figures depicting the lateral drift 5.20, 5.1, 5.22 are pretty much the same as for the axial case, as the system is able to keep up with the change in position.

Chapter 6

Discussion

The objective of this thesis has been to investigate the use of position control in inductive power transfer and how it compares to the state-of-the-art methods for inductive power transfer control. It has been attempted to meet the objective through the work as documented in this report:

- Basic principles for the design and control of IPT systems for high power applications (Chapter 2)
- Magnetic field for a thin circular coil and mutual inductance between two thin circular coils (Chapter 3)
- Transfer functions for SS compensated IPT systems for CR and CV load (Chapter 4)
- Demonstrate position control for lateral and transversal displacement of the receiving coil relative to the transmitter (Chapter 5)

In this chapter we will go through the results and discuss the validity of the work done.

Magnetic field and Mutual Inductance

The most important relationship required for position control in IPT is how the coupling coefficient or mutual inductance varies with position. We have modelled the magnetic field from a thin circular wire for this purpose, and this choice is a compromise between computational simplicity and relevance. The magnetic field from a circular loop can be expressed in closed form as a weighted sum of elliptic integrals and has been known for years Simpson et al. (24). We have calculated and implemented, in Matlab, the magnetic

field for two reasons. One is that the magnetic field gives and indication of the possible variations in the mutual inductance. The other reason is that it can be used to verify the calculation of the magnetic flux and thus the mutual inductance, as will be explained shortly.

The mutual inductance between two circular coils is much more complicated to calculate than the magnetic field, and only the case with coaxial loops is known in closed form. One result from this thesis is that we have developed an approximate expressions that is valid for small distances between the two coils. A model has been developed for two special cases: for relative coaxial movement along the axis of symmetry and relative movement of the receiver in a plane parallel to the transmitter plane. In the model presented here, the two coils don't need to be equal size. Since the mutual inductance is sort of the average magnetic field on a surface, we recreate the magnetic field from the mutual inductance by considering a very small receiver.

What are the limitations of the calculations done? Here are a few:

Thin wire approximation - One very common assumption to make, which have been adopted here, is to neglect the size (cross section) of the wire when calculating the magnetic field from wires . This assumption breaks down close to the wire, and therefore the results obtained are not valid (very) close to the wire.

Simple and decoupled movements only - The axial and lateral movements are evaluated independently of one another. For the lateral displacement case only displacement in one direction is considered, though the two possible lateral displacements directions are equal, and a combination of the two can modeled as a sum of the individual movements. The combination case of a lateral and axial displacement at the same time has not been considered. Though it can be intuitively understood from figure 3.6 and A.12 that a lateral displacement will have more dire consequences when the primary and secondary coils are close to one another. Nevertheless the system only considers that the mechanical system only needs to move in one direction. This might also be a beneficial design choice, as developing a movable mechanical system with one degree of freedom is considerably easier than one with three or six. As such one could regulate only the degree of freedom that is the most susceptible to change in position during charging conditions.

Angular Displacement has not been considered Time did not permit this thesis to include considerations of movements other than coaxial

and transversal movements parallel to the transmitter plane. One possible mode is that the receiver oscillates slowly around an axis parallel to the transmitter plane. The coupling coefficient is rather resistant to changes in angular alignment, and it is likely that a relatively good estimate of the effect is obtained by considering the effective area of the receiver. It is likely, that the angular displacement has to be quite severe in order to have big impact on the output power. Having a position control system for this operation would require considerably more engineering, than for the other two cases of misalignment.

Simple magnetic arrangements - We have seen how sensitive the mutual inductance is to changes in distance close to the transmitter trough 3.6 and A.12. As explained earlier, it is important to remember that this is for just one coil and only one turn. The mutual inductance can be made less directionally dependent if the magnetic configuration of the system is improved, by the use of advanced high quality coils and advanced magnetic design.(10)

What are the consequences of these limitations? In the far field, where the detailed geometry of the sender is less important, there are few obvious consequences. In the near field the consequences are thought to be significant and many, but the only way to know is to measure the mutual inductance for a realistic magnetic arrangement.

Transfer functions

The mathematical expressions for the various transfer functions for an SS-compensated IPT system from the basic circuit equations have been derived. These expressions have been implemented in Matlab, and we are now able to calculate transfer functions and power output for any SS compensated IPT system with CR or CV load. The transfer functions for the lossless case has been verified by comparing our results with the result from (18). Without access to the expression for the transfer functions for the lossy case, the results have been verified by comparing plots of transfer functions with corresponding ones in the aforementioned paper. One example is 4.8 and figure 5 in (18).

Position control

A very basic negative-feedback controller has been implemented. The need for advanced control may arise in practical implementations, but has to be tailor made to the specific applications. A more advanced controller requires knowledge of the actuating component responsible for the movement, as their inertia and speed are essential. Simulations have been presented of the system response for three typical deviations that are experienced in other control applications:

Sudden change in position - The step function corresponds to a sudden shift in position. We saw it has a large impact on the coupling coefficient, as expected.

Slow moving wave - A sine wave is used as a crude simulation of a scenario where the primary coil is able to change it's position to some control input. The secondary coil is affected by some environmental effect, and has it's position altered as a result. One example is small waves impacting a boat with the receiver on board. The receiver moves back and forth because of the waves, creating misalignment between the two coils. This movement is represented as a sine signal with some gaussian white noise added to it. This is of course a crude simplification of wave dynamics,thou for the scope of this thesis, it is sufficient. The noise has been added to show how measurement noise has a cascading effect on the system. The coupling coefficient is very sensitive to movement, in particular in the near field. Since the power delivered to the load depends on the square of the the coupling the noise will be further amplified.

Gradual change in position - The ramp function is used as a base case to compare against the results of Guidi and Suul (18), who looked at 275 % change in coupling coefficient over a short time span.

Practical use of position control for IPT

Inductive power transfer applications ranges from battery charging of small moving objects (i.e. drones and mobile robots) to battery charging of cars and ferries. It goes without saying that the requirements with regards to cost, payload, position measurements, actuators etc are hugely different in the two cases. What are the issues that determines the viability of position controlled IPT systems compared to conventional IPT systems?

Position measurements - It is obvious from the earlier discussions that position measurements are vital for an IPT position control system. If we assume that we have control of the transmitter position, we still need in the more general case to obtain 6 degrees of freedom (DOF) for the receiver either by direct measurements or by receiving the position from the receiver. This may not always be that easy to obtain, and there may be very different measurement precision's for the different DOFs. This situation may be alleviated by the fact that in some cases not all DOFs are needed, and that the major variation in position is in one or two directions only. Analysis and decoupling of the possible movement of the receiver will thus be an important design activity. Some DOFs may have a larger impact on efficiency than other, at it may be possible to eliminate the need for control of some DOFs by carefully designing the shape of the transmitter and receiver.

Actuators - One rather obvious disadvantage with position control is that it includes moving mechanical parts, which are more prone to wear and tear. If it is required to move large masses around, and large accelerations are necessary, the needed equipment will be quite bulky and expensive. Moreover, large actuators able to move large masses also requires additional safety measures. If relative motion in only one direction is required, things may different.

Cost - Without a specific application, no attempts have been made to compare cost between a traditional IPT system and a position controlled system. One design criteria for traditional system is trying to avoid bulky and expensive converters. However, this argument may be used against position control since it is reasonable to assume that the cost of the actuators will be rather high for high power applications.

Comparison - What to choose?

It may be possible to attain a higher efficiency using position control, than that of the approach in (18) because the quality factor can be increased further, the operational frequency kept constant and the bandwidth reduced. However, a necessary requirement is that we are able to control the position of the receiver. As has been discussed, this may or may not be possible, and only a detailed analysis of the specific application can decide between the two approaches. This approach is also susceptible to component degradation. My personal opinion is that for most high power applications, the state-

of-the art solution described is better by far. If one has access to position measurements, it is probably better to use these measurements for predicting movements and use the resulting predictions to further improve the current and frequency control.

Chapter 7

Conclusion

The ability to optimize the efficiency of an IPT system, by maintaining the most influential variable, the coupling coefficient at a constant optimum, has been investigated. With operations in the nearfield region the mutual inductance is highly volatile, both for axial and lateral movement. Maintaining a constant reference position in this region imposes demanding requirements on both the controlling unit and the mechanical apparatus responsible for the physical movement. The farfield operation, however, is more forgiving. Regardless, complete system analysis has to be done for each specific implementation, as the inertia of the system and the input dynamics must be known. The reference input has to be followed as closely as possible in order to maintain high efficiency. The added cost of implementing and maintaining such a system has also to be considered. As such position control can be a valid solution in certain cases where the correct conditions are present. My personal opinion is that for most high power applications, the state-of-the art solution described by Guidi and Sul is better by far for most high power applications. Tight position control may still have its niche applications.

Future Work

As has been discussed throughout this work, the use of position control has to be decided on a case-by-case basis. Any future work need to consider a specific application in order to get reliable information regarding the most important parameters: position measurements, actuators and life-cycle costs. Another line of future work is to continue the work of modelling the mutual inductance for general relative movement and try to find approximative solutions that can be used for simpler design of new systems.

Bibliography

[1] Akyel, C., Babic, S. I., and Mahmoudi, M.-M. (2009). Mutual inductance calculation for noncoaxial circular air coils with paralell axes. *Progress In Electromagnetics Research*, 91:287 – 301.

[2] Anele, A. O., Hamam, Y., Chassagne, L., Alayli, J. L. Y., and Djouani, K. (2015). Evaluation of the magnetic fields and mutual inductance between circular coils arbitrarily positioned in space. *4th International Conference on Mathematical Modeling in Physical Sciences*.

[3] Barman, S., Reza, A., Kumar, N., Karim, E., and Munir, A. (2015). Wireless powering by magnetic resonant coupling: Recent trends in wireless power transfer system and its applications. *Renewable and Sustainable Energy Reviews*, pages 1525–1552.

[4] Bateman, H. (1953). Higher transcendental functions. 2:295 – 322.

[5] Bosshard, R., Kolar, J. W., Mühlethaler, J., Stevanović, I., Wunsch, B., and Canales, F. (2015). Modeling and η-α-pareto optimization of inductive power transfer coils for electric vehicles. *IEEE Journal of Emerging and Selected Topics in Power Electronics*, 3(1).

[6] Boys, J. T., Covic, G. A., and A.W.Green (2000). Stability and control of inductively coupled power transfer systems. *IEEE Proc.-Electr. Power Appl.*, 147(1).

[7] Brecher, A. and Arthur, D. (2014). Review and evaluation of wireless power transfer (wpt) for electric transit applications. *FTA Report No. 0060*.

[8] Chan, H., Cheng, K. W., and Sutanto, D. (2000). A simplified neumann's formula for calculation of inductance of spiral coil. In *Power Electronics and Variable Speed Drives, 18-19 September 2000, Conference Publication*.

[9] Chen, C.-T. (2013). *Linear System Theory and Design*. Oxford University Press.

[10] Covic, G. and Boys, J. (2013a). Modern trends in inductive power transfer for transport applications. *IEEE Journal of Emerging and selected topics in power electronics*, 1(1).

[11] Covic, G. A. and Boys, J. T. (2013b). Inductive power transfer. *Proceedings of the IEEE*, 101(6).

[12] Diekhans, T. and Doncker, R. W. D. (2015). A dual-side controlled inductive power transfer system optimized for large coupling factor variations and partial load. *IEEE Transaction on Power Electronics*, 30(11).

[13] Fernández, C., Garcia, O., Prieto, R., Cobos, J. A., and Uceda, J. (2002). Overview of different alternatives for the contact-less transmission of energy. *IECON 02 IEEE 2002 28th Annual Conference of the Industrial Electronics Society.*

[14] Feynman, R. P. (2010). The feynman lectures on physics. pages 14.1 – 16.10.

[15] Fotopoulou, K. and Fly, B. W. (2011). Wireless power transfer in loosely coupled links: Coil misalignment model. *IEEE Transactions on Magnetics*, 47(2).

[16] Garnica, J. and Lin, R. A. C. J. (2013). Wireless power transmission: From far field to near field. *Proceedings of the IEEE*, 101(6).

[17] Guidi, G. (2015). Power flow control of inductive power transfer systems for wireless battery charger. *SINTEF Project Memo AN 14.12.82.*

[18] Guidi, G. and Suul, J. A. (2016). Minimizing converter requirements of inductive power transfer systems with constant voltage load and variable coupling conditions. *IEEE Transaction on Industrial Electronics*, 63(11).

[19] Imura, T. and Hori, Y. (2011). Maximizing air gap and efficiency of magnetic resonant coupling for wireless power transfer using equivalent circuit and neumann formula. *IEEE Transactions on Industrial Electronics*, 58(10).

[20] Jackson, J. D. (1975). Classical electrodynamics. pages 168 – 209.

[21] Kurs, A. (2007). Wireless power transfer via strongly coupled magnetic resonances. *Science*, 317.

[22] Li, S. and Mi, C. C. (2015). Wireless power transfer for electric vehicle applications. *IIEEE Journal of Emerging and Selected Topics in Power Electronics*, 3(3).

[23] Mur-Miranda, J. O., Fanti, G., Feng, Y., Omanakuttan, K., Ongie, R., Setjoadi, A., and Sharpe, N. (2010). Wireless power transfer using weakly coupled magnetostatic resonators. *IEEE Energy Conversion Congress and Exposition (ECCE)*.

[24] Simpson, J., Lane, J., Immer, C., and Youngquist, R. (2001). Simple analytic expression for the magnetic field of a circular current loop.

[25] Soma, M., Galbraith, D. C., and White, R. L. (1987). Radio-frequency coils in implantable devices: Misalignment analysis and design procedure. *IEEE Transaction on Biomedical Engineering*, BME-34(4).

[26] Steigerwald, R. L. (1988). A comparison of half-bridge resonant converter topologies. *IEEE Transaction on Power Electronics*, 3(2).

[27] T, S. (2017). Fra sommeren vil bilfergen lades med induksjon.

[Takanashi et al.] Takanashi, H., Y.Sato, Y.Kaneko, S.Abe, and Yasuda, T. A large air gap 3 kw wireless power transfer system for electric vehicles. *IEEE Eneregy Convers. Congr. Exposit*, pages 269 – 274.

[29] Wang, C., Covic, G. A., and Stielau, O. H. (2004). Power transfer capability and bifurcation phenomena of loosely coupled inductive power transfer systems. *IEEE Transactions on Industrial Electronics*, 51(1).

[30] Wang, C., Stielauand, O. H., and Covic, G. A. (2005). Design consideration for a contactless electric vehicle battery charger. *IEEE Transactions on Industrial Electronics*, pages 1308 – 1314.

Appendix A

Magnetic field and Mutual Inductance

There are two simple, interrelated, physic principles that forms the basis for inductive power transfer. Firstly, when a charged particle is moving in space, it produces a magnetic field. A current, which is a flow of charged particles, will thus generate a magnetic field. Furthermore, a magnetic field exerts a force on a moving charged particle and a magnetic field may thus generate a voltage in an electric circuit. The basic principle behind inductive power transfer is to use a primary electric circuit to generate a magnetic field which in turn induces a voltage in a secondary electric circuit some distance away from the primary circuit.

A.1 Formulas for calculating mutual inductance

The magnetic flux and the mutual inductance may be calculated in various ways, and the starting point for calculations varies a lot in the literature. We will here give a summary of relevant formulas and approaches for calculating the flux through a surface and the corresponding mutual inductance. We will also, in some detail, show the results from the calculation of magnetic field from a circular wire and the results from calculating the mutual inductance between two wires. For further details the reader is referred to Jackson (20) and Feynman (14).

A.1.1 Calculating flux from the magnetic field

If $\vec{\boldsymbol{B}}(\vec{r}, t)$ is known, calculating the magnetic flux requires calculating a double integral. If the magnetic field is not known, the magnetic field from a source current density $\vec{\boldsymbol{j}}(\vec{r}_0)$ in a volume V can be calculated from Biot and Savarts law:

$$\vec{\boldsymbol{B}}(\vec{r}) = \frac{\mu_0}{4\pi} \int_V \frac{\vec{\boldsymbol{j}}(\vec{r}_0) \times (\vec{\boldsymbol{r}} - \vec{\boldsymbol{r}}_0)}{|\vec{\boldsymbol{r}} - \vec{\boldsymbol{r}}_0|^3} d^3 r_0 \tag{A.1}$$

A.1.2 Calculating flux from the vector potential

Instead of calculating the magnetic field directly, it is sometimes more convenient to first calculate the vector potential $\vec{\boldsymbol{A}}(\vec{r}_0)$ related to the magnetic field through

$$\vec{\boldsymbol{B}}(\vec{r}) = \nabla \times \vec{\boldsymbol{A}}(\vec{r}) \tag{A.2}$$

and it can be shown that from Biot-Savarts law we get for the vector potential:

$$\vec{\boldsymbol{A}}(\vec{r}) = \frac{\mu_0}{4\pi} \int_V \frac{\vec{\boldsymbol{j}}(\vec{r}_0)}{|\vec{\boldsymbol{r}} - \vec{\boldsymbol{r}}_0|} d^3 r_0 \tag{A.3}$$

The magnetic flux through a surface Ω is:

$$\Phi(t) = \int_\Omega \nabla \times \vec{\boldsymbol{A}}(\vec{r}, t) \cdot \vec{\boldsymbol{dS}} \tag{A.4}$$

Using Stoke's theorem we can convert the surface integral in A.4 to a line integral over the enclosing curve:

$$\Phi(t) = \oint_\Gamma \vec{\boldsymbol{A}}(\vec{r}, t) \cdot \vec{\boldsymbol{dl}} \tag{A.5}$$

A.1.3 Thin wire approximation

We will in this thesis only consider wires where the shape and dimension of the cross section is very small compared to the length of the wire. To be more specific, we consider a wire with circular cross sectional radius δ carrying a current I. (The exact shape of the cross section is not important in this context) It is reasonable to assume that if the radius is small enough, the current density is constant over the cross section:

$$\vec{\boldsymbol{j}}(\vec{\boldsymbol{r}}_0) = \frac{I}{\pi \delta^2} \vec{\boldsymbol{e}}_0 \tag{A.6}$$

, where $\vec{\boldsymbol{e}}_{\mathbf{0}}$ is a unit vector tangential to the wire. Using eq. A.6 in eq. A.3, the integration over the cross section is now trivial and we are left with:

$$\vec{\boldsymbol{A}}(\vec{r}) = \frac{\mu_0 I}{4\pi} \int_\Gamma \frac{1}{|\vec{\boldsymbol{r}} - \vec{\boldsymbol{r}}_0|} \vec{\boldsymbol{dl}}_{\mathbf{0}} \tag{A.7}$$

, where $\vec{\boldsymbol{dl}}_{\mathbf{0}}$ is a line element tangential to the wire.

Mutual inductance with the thin wire approximation Using the expression for $\vec{\boldsymbol{A}}(\vec{r}, t)$ for a very thin wire, the magnetic flux becomes:

$$\Phi(t) = \frac{\mu_0 I}{4\pi} \oint_{\Gamma_2} \oint_{\Gamma_1} \frac{\vec{\boldsymbol{dl}}_{\mathbf{1}} \cdot \vec{\boldsymbol{dl}}_{\mathbf{2}}}{|\vec{\boldsymbol{r}} - \vec{\boldsymbol{r}}_0|} \tag{A.8}$$

Realizing that I is the only time varying variable in eq. A.8 we get

$$\varepsilon(t) = -\frac{\mu_0}{4\pi} \frac{dI}{dt} \oint_{\Gamma_2} \oint_{\Gamma_1} \frac{\vec{\boldsymbol{dl}}_{\mathbf{1}} \cdot \vec{\boldsymbol{dl}}_{\mathbf{2}}}{|\vec{\boldsymbol{r}} - \vec{\boldsymbol{r}}_0|} \tag{A.9}$$

and finally

$$M = \frac{\mu_0}{4\pi} \oint_{\Gamma_2} \oint_{\Gamma_1} \frac{\vec{\boldsymbol{dl}}_{\mathbf{1}} \cdot \vec{\boldsymbol{dl}}_{\mathbf{2}}}{|\vec{\boldsymbol{r}} - \vec{\boldsymbol{r}}_0|} \tag{A.10}$$

, which is the Von Neumann formula for the mutual inductance between two loops Γ_1 and Γ_2. For finding the mutual inductance between two circular loops, we choose to first calculate the vector potential generated by the primary loop by using eq. A.7 and then calculate the flux through the second loop by using eq. A.5. The added value of this approach is that when the vector potential has been calculated, it is easy to calculate the magnetic field through differentiation.

A.2 Magnetic field from circular current loop

A.2.1 Vector potential for a circular loop

We will calculate the vector potential for a conducting circular wire with radius a, with center in origo carrying a current I as shown in figure A.1. In eq. A.7, $\vec{\boldsymbol{dl}}_{\mathbf{0}} = a d\theta \vec{\boldsymbol{e}}_{\boldsymbol{\theta}_{\mathbf{0}}}$, and we get:

$$\vec{\boldsymbol{A}}(\vec{r}) = \frac{\mu_0 a I}{4\pi} \int_0^{2\pi} \frac{1}{|\vec{\boldsymbol{r}} - \vec{\boldsymbol{r}}_0|} d\theta \vec{\boldsymbol{e}}_{\boldsymbol{\theta}_{\mathbf{0}}} \tag{A.11}$$

Here

$$|\vec{r} - \vec{r}_0| = \sqrt{(x - x_0)^2 + (y - y_0)^2 + z^2}$$
$$= \sqrt{x^2 + y^2 + z^2 + a^2 - 2axcos\theta_0 - 2aysin\theta_0} \quad \text{(A.12)}$$
$$\vec{e}_{\theta_0} = -sin\theta_0\vec{i} + cos\theta_0\vec{j} \quad \text{(A.13)}$$

, where $\vec{i}$ and $\vec{j}$ are the unit vectors in the x- and y-direction, respectively.

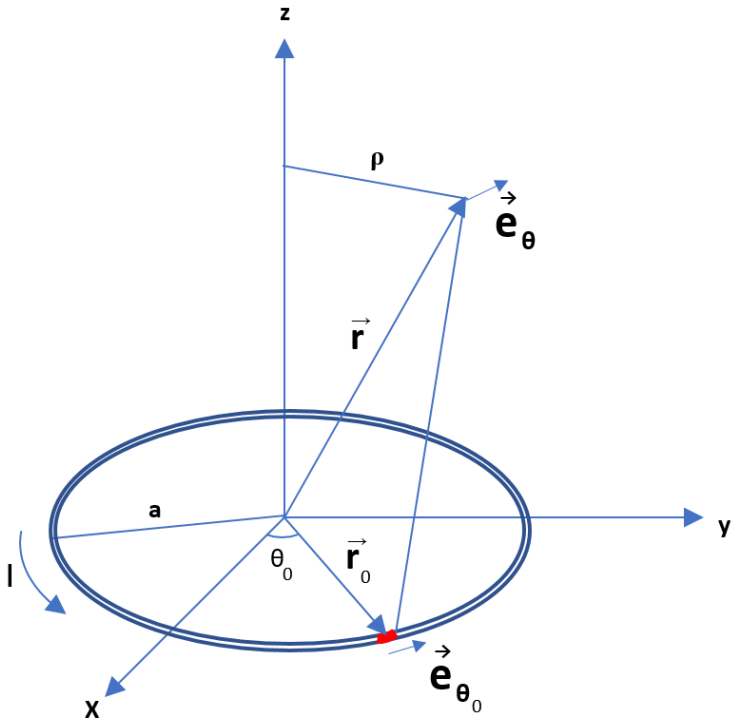

Figure A.1: Schematic coordinate system for calculating vector potential for a circular loop

It is evident that the vector potential and thus the magnetic field has to be symmetric around the z-axis. We can therefore choose y=0 in (15), and (14) takes the form:

$$\vec{A}(\vec{r}) = \frac{\mu_0 aI}{4\pi}\int_0^{2\pi} \frac{-sin\theta_0\vec{i} + cos\theta_0\vec{j}}{\sqrt{x^2 + z^2 + a^2 - 2axcos\theta_0}} d\theta_0 \quad \text{(A.14)}$$

Since $sin\theta_0$ is anti-symmetric about $\theta_0 = 0$, the integral along $\vec{i}$ is zero and we are left with:

$$\vec{A}(\vec{r}) = \frac{\mu_0 aI}{4\pi}\vec{j}\int_0^{2\pi} \frac{cos\theta_0}{\sqrt{x^2 + z^2 + a^2 - 2axcos\theta_0}} d\theta_0 \quad \text{(A.15)}$$

One final transformation is to convert (18) back from a point in the xz plane, $(x, 0, z)$ to a random point (ρ, θ, z). This is obtained by the transformation $y \longrightarrow \rho$ and $\vec{\boldsymbol{j}} \longrightarrow \vec{\boldsymbol{e}}_{\boldsymbol{\theta}}$, which gives:

$$\vec{\boldsymbol{A}}(\vec{r}) = \frac{\mu_0 a I}{4\pi}\vec{\boldsymbol{e}}_{\boldsymbol{\theta}} \int_0^{2\pi} \frac{cos\theta_0}{\sqrt{\rho^2 + z^2 + a^2 - 2a\rho cos\theta_0}} d\theta_0 \tag{A.16}$$

Using eq. (28) with $c = \rho^2 + z^2 + a^2$ and $d = 2a\rho$, we get:

$$\vec{\boldsymbol{A}}(\vec{r}) = \frac{\mu_0 a I}{4\pi}\vec{\boldsymbol{e}}_{\boldsymbol{\theta}} \frac{2\sqrt{(\rho + a)^2 + z^2}}{a\rho} \left(\frac{\rho^2 + a^2 + z^2}{(\rho + a)^2 + z^2} K(m) - E(m)\right) \tag{A.17}$$

, where we have defined

$$m^2 = \frac{4\rho a}{(\rho + a)^2 + z^2} \tag{A.18}$$

A more convenient form of eq. (20) is:

$$\vec{\boldsymbol{A}}(\vec{r}) = \frac{\mu_0 I}{4\pi} 2\sqrt{\frac{a}{\rho}} \frac{(2 - m^2)K(m) - 2E(m)}{m} \vec{\boldsymbol{e}}_{\boldsymbol{\theta}} \tag{A.19}$$

or

$$\vec{\boldsymbol{A}}(\vec{r}) = \frac{\mu_0 I a}{\pi\sqrt{(\rho + a)^2 + z^2}} \frac{(2 - m^2)K(m) - 2E(m)}{m^2} \vec{\boldsymbol{e}}_{\boldsymbol{\theta}} \tag{A.20}$$

A.2.2 Magnetic Field from a circular loop

The magnetic field from a a circular loop carrying a current I may be calculated from eq. A.2. The vector potential $\vec{\boldsymbol{A}}(\vec{r})$ given by eq. A.20, and in cylindrical coordinates $A_\rho(\vec{r}) = A_z(\vec{r}) = 0$, and the magnetic field is

$$\vec{\boldsymbol{B}}(\vec{r}) = -\frac{\partial A_\theta(\rho, z)}{\partial z}\vec{\boldsymbol{e}}_{\boldsymbol{\rho}} + \frac{1}{\rho}\frac{\partial}{\partial \rho}(\rho A_\theta(\rho, z))\vec{\boldsymbol{e}}_{\boldsymbol{z}} \tag{A.21}$$

or

$$B_\rho(\rho, z) = -\frac{\partial A_\theta(\rho, z)}{\partial z} \tag{A.22}$$

$$B_\theta(\rho, z) = 0 \tag{A.23}$$

$$B_z(\rho, z) = \frac{1}{\rho}\frac{\partial}{\partial z}(\rho A_\theta(\rho, z)) \tag{A.24}$$

Calculating B_ρ and B_z, using the expression for the derivative of elliptic integrals given in eq. A.66-A.67 is quite straightforward but rather lengthy and is omitted here. We will only give the results in cylindrical coordinates:

$$B_\rho(\rho, z) = \frac{Cz}{2\alpha^2\beta\rho}[\frac{\alpha^2 + \beta^2}{2}E(m) - \alpha^2 K(m)] \tag{A.25}$$

$$B_z(\rho, z) = \frac{C}{2\alpha^2\beta}[\alpha^2 K(m) + (a^2 - \rho^2 - z^2)E(m)] \tag{A.26}$$

, where

$$C = \frac{\mu_0 I}{\pi} \tag{A.27}$$

$$\alpha^2 = (a - \rho)^2 + z^2 \tag{A.28}$$

$$\beta^2 = (a + \rho)^2 + z^2 \tag{A.29}$$

$$m^2 = \frac{4a\rho}{(a + \rho)^2 + z^2} = 1 - \frac{\alpha^2}{\beta^2} \tag{A.30}$$

In (24) the magnetic field from a circular loop for both cylindrical, rectangular and spherical coordinates. In addition they have calculated explicit formulas for the spatial derivatives of the magnetic field, which may be handy if linearization is needed.

The axial magnetic field (in the z-direction) for a circular loop as a function of distance from the symmetry axis is shown in Figure A.6 for distances not too far from the loop. It is seen that close to the plane of the loop the axial field changes rather abruptly close to the wire. It is seen that the magnetic field switches direction from the positive z-direction to the negative. The

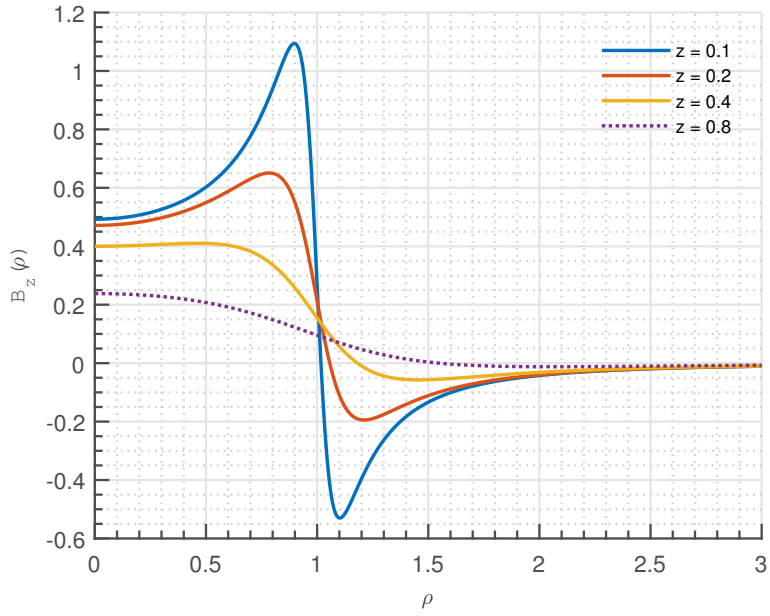

Figure A.2: Axial magnetic field as a function of distance from the symmetry axis for 4 distances along the axis: $z = 0.1a, 0.2a, 0.4a$ and $0.8a$

distance from the axis where the change of direction happens is $\rho = a$ at the wire plane, and increases the further away from the axis one moves. If we consider the magnetic flux through another coaxial circular shaped wire loop in a plane parallel to the xy-plane, it will be positive. However, if we move this coil further and further away from the axis in the near field the flux will at some distance become negative.

The axial field (in the z-direction) further away from the loop plane is shown in Figure A.3. It is seen that the magnetic field changes more smoothly with distance from the axis, but it still becomes negative some distance from the axis.

The radial magnetic field is shown in Figures A.4 and A.5 for the same distances as for the axial field. For distances close to the loop, the radial field is sharply peaked around$\rho = a$ and above. For later use, from A.25 the on-axis magnetic field is:

$$B_z(0, z) = \frac{\mu_0 I a^2}{2(a^2 + z^2)^{\frac{3}{2}}} \tag{A.31}$$

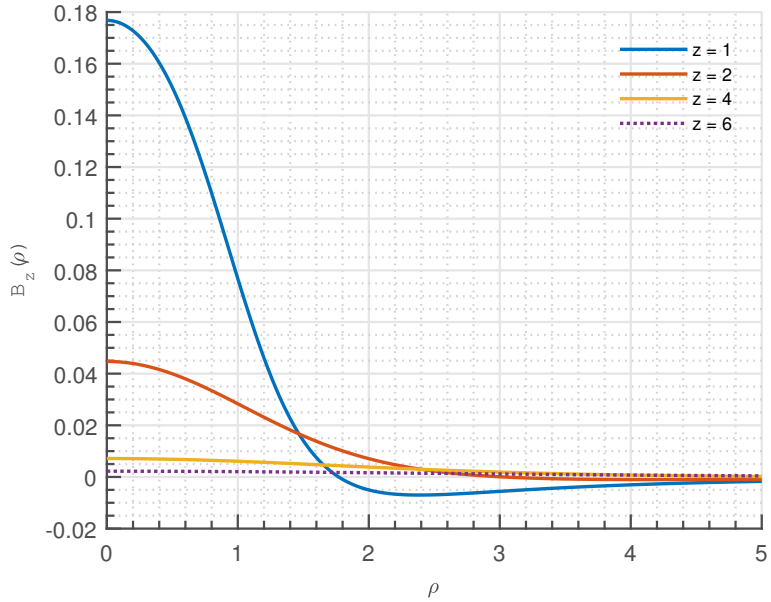

Figure A.3: Axial magnetic field as a function of distance from the symmetry axis for 4 distances along the axis: $z = a, 2a, 4a$ and $6a$

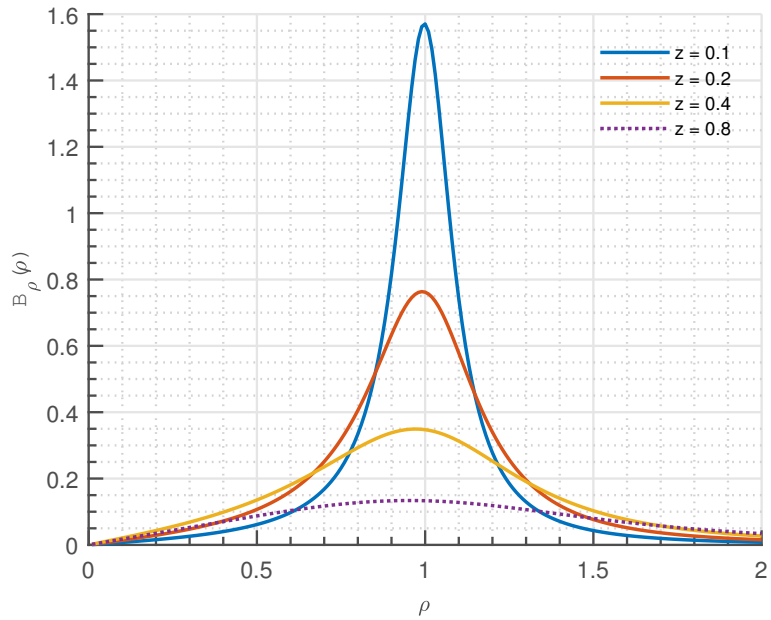

Figure A.4: Radial magnetic field as a function of distance from the symmetry axis for 4 distances along the axis: $z = 0.1a, 0.2a, 0.4a$ and $0.8a$

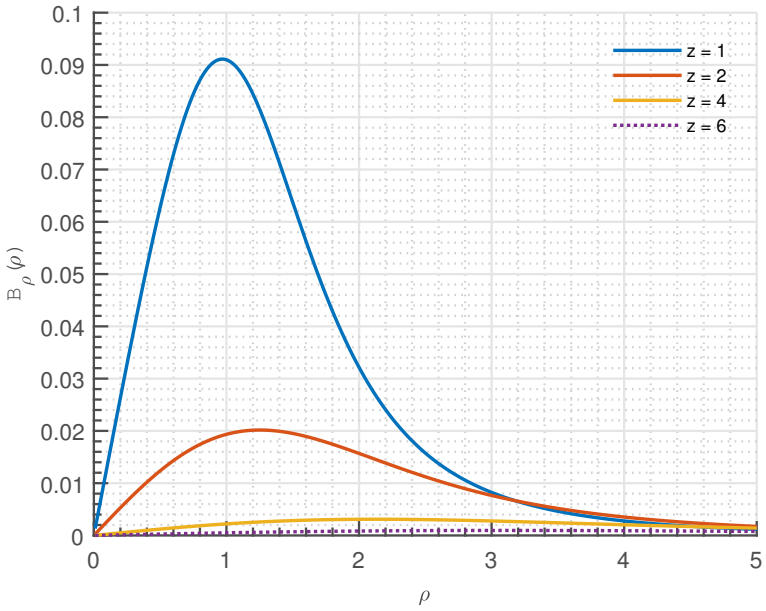

Figure A.5: Radial magnetic field as a function of distance from the symmetry axis for 4 distances along the axis: $z = a, 2a, 4a$ and $6a$

A.3 Mutual Inductance between circular loops

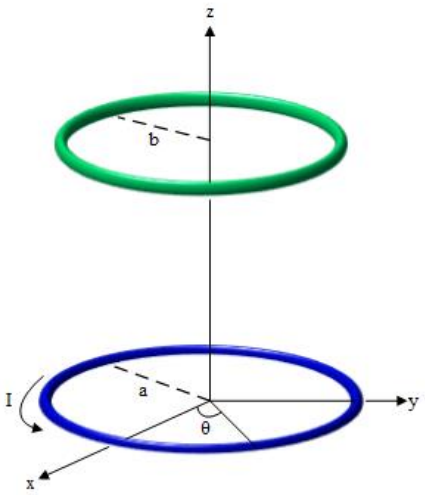

Figure A.6: Coil arrangement for coaxial loops

A.3.1 Coaxial loops

We consider the mutual inductance between two concentric circular loops. The first loop, the transmitter, has radius a and is located in the xy plane, centered at origin. The second loop, the receiver, with a radius b is located in a plane parallel to and a distance z away from the xy plane. We are interested in the mutual inductance between the two loops caused by a current I in the first loop. The vector potential from the transmitter is given by eq. A.20. At the receiver, $\rho = b$, and the vector potential is:

$$\vec{\boldsymbol{A}}(\vec{r}) = \frac{\mu_0 I a}{\pi\sqrt{(a+b)^2+z^2}} \frac{(2-m^2)K(m) - 2E(m)}{m^2} \vec{\boldsymbol{e}}_{\boldsymbol{\theta}} \tag{A.32}$$

with

$$m^2 = \frac{4ab}{(a+b)^2+z^2} \tag{A.33}$$

In eq. A.5 $\vec{\boldsymbol{dl}} = bd\theta\vec{\boldsymbol{e}}_{\boldsymbol{\theta}}$, and the integration is trivial. The flux is

$$\Phi(t) = \frac{2\mu_0 Iab}{\sqrt{(a+b)^2+z^2}} \frac{(2-m^2)K(m) - 2E(m)}{m^2} \tag{A.34}$$

, and the mutual inductance for two coaxial circular loops is

$$M = \frac{2\mu_0 ab}{\sqrt{(a+b)^2+z^2}} \frac{(2-m^2)K(m) - 2E(m)}{m^2} \tag{A.35}$$

Now we define:

$$\Gamma(m) = \frac{(2-m^2)K(m) - 2E(m)}{m^2} \tag{A.36}$$

By introducing the power series for $K(m)$ and $E(m)$ in eq. A.36, we obtain the following two first and second order approximations for the mutual inductance:

$$M_1 = \frac{\pi\mu_0(ab)^2}{2[(a+b)^2+z^2]^{\frac{3}{2}}} \tag{A.37}$$

$$M_2 = \frac{\pi\mu_0(ab)^2}{2[(a+b)^2+z^2]^{\frac{3}{2}}} \left[1 + \frac{3ab}{(a+b)^2+z^2}\right] \tag{A.38}$$

The first approximation is obtained by retaining the first non-vanishing term in the series expansions. If we divide with πb^2, set $b = 0$ and multiply with I, we end up with the magnetic field on axis given by A.26. (The magnetic flux through a surface divided by the surface area is equal to the average magnetic field over the surface.)

In figure A.7 the mutual inductance as a function of separation between two equal-sized circular coils is shown. In addition, the two approximative expressions from eq. A.37 and A.38 are included. It is seen that in the nearfield neither of the two expressions are close to the exact solution. This is also shown in figure A.8 where the relative error for the two approximate expressions are shown.

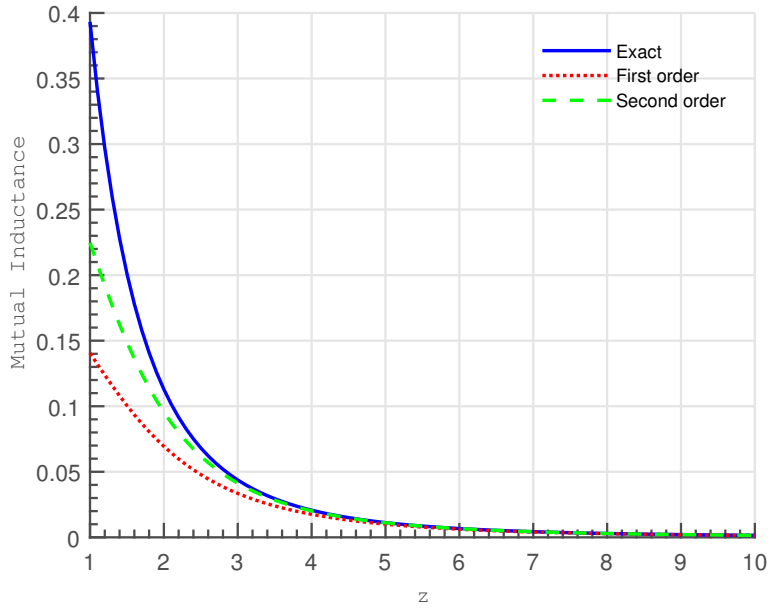

Figure A.7: Mutual inductance between two coaxial, equal sized coils as a function of separation between them. In addition to the exact expression for the mutual inductance, the first (non-vanishing) and second order approximations are included.

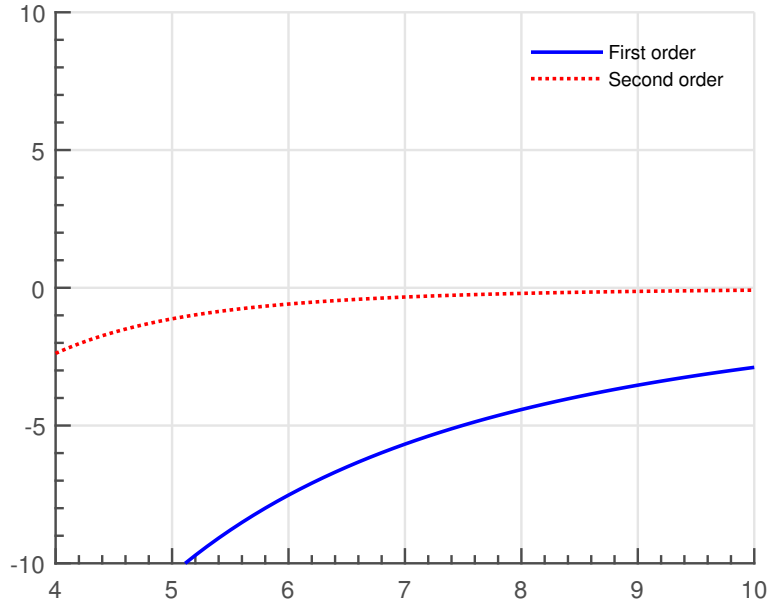

Figure A.8: Relative error by using the first and the second order approximation for the mutual inductance between two coaxial, equal sized coils as a function of separation

We are now going to find another approximate expression for the mutual inductance that is valid for smaller separation. We start with eq. A.36 with

$$m^2 = 1 - \frac{\alpha^2}{\beta^2} \tag{A.39}$$

$$\alpha^2 = (a-b)^2 + z^2 \tag{A.40}$$

$$\beta^2 = (a+b)^2 + z^2 \tag{A.41}$$

$$m' = \sqrt{1-m^2} = \frac{\alpha}{\beta} \tag{A.42}$$

We will reformulate the expression for $\Gamma(m)$ using eq. A.75 and A.76 with the definitions above. This is quite straightforward, but lengthy and only the result is shown here:

$$\Gamma(m) = \frac{2\beta}{\beta-\alpha}\Big[K\Big(\frac{\beta-\alpha}{\beta+\alpha}\Big) - E\Big(\frac{\beta-\alpha}{\beta+\alpha}\Big] \tag{A.43}$$

and the mutual inductance is:

$$M = \frac{4\mu_0 ab}{\beta+\alpha}\frac{K\left(\frac{\beta-\alpha}{\beta+\alpha}\right) - E\left(\frac{\beta-\alpha}{\beta+\alpha}\right)}{\frac{\beta-\alpha}{\beta+\alpha}} \tag{A.44}$$

If we now expand the elliptic integrals we get:

$$M_1 = \frac{4\pi\mu_0(ab)^2}{(\beta+\alpha)^3} \tag{A.45}$$

$$M_2 = \frac{\mu_0\pi ab(\beta-\alpha)}{(\beta+\alpha)^2}\left(1 + 6\frac{a^2b^2}{(\alpha+\beta)^4}\right) \tag{A.46}$$

Comparing eq. A.37 and A.46 shows that the effect of the transformation is to replace β with an average of β and α. The two approximations are shown in figure A.9 and A.10.It is senn that the improvement is significant and even the first order approximation is valid for separation of one radius and above.

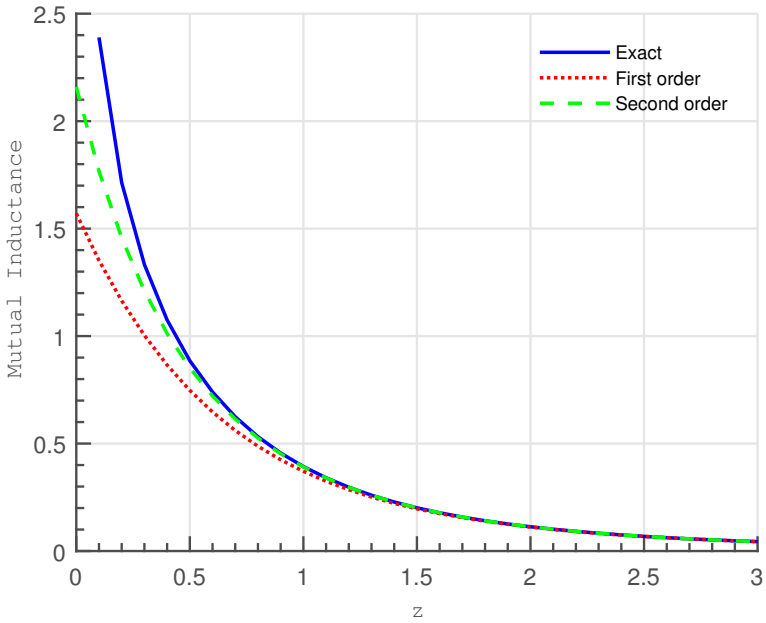

Figure A.9: Mutual inductance between two coaxial, equal sized coils as a function of separation. The first (non-vanishing) and second order new approximations are included.

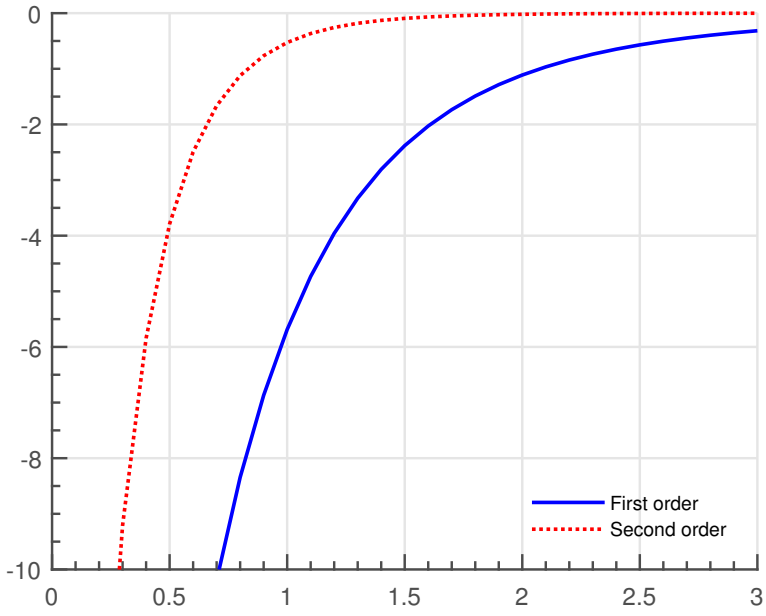

Figure A.10: Relative error by using the new first and the second order approximation for the mutual inductance between two coaxial, equal sized coils as a function of separation

A.3.2 Lateral displaced loops

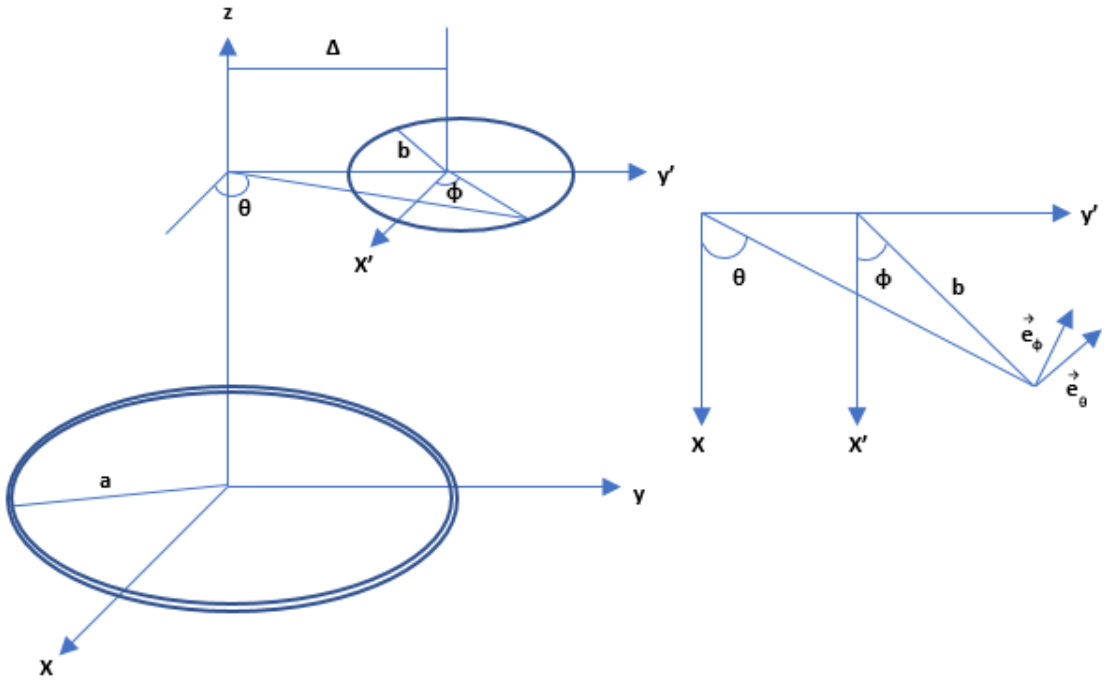

Figure A.11: Coil with lateral displacement. The receiving coil is displaced a distance Δ form the axis at a distance Z from the transmitting coil. To the right is a projection of the geometry to the xy plane.

Again we consider two circular coils, the transmitter with radius a and center in origo, and the receiver with radius b in a plane parallel to the xy-plane. The receiver is an axial distance z from the transmitter and is displaced laterally a distance Δ. The configuration is shown in A.11. From the figure we have the following relations:

$$x' = b\cos(\phi) \tag{A.47}$$

$$y' = b\sin(\phi) \tag{A.48}$$

$$\rho = \sqrt{x'^2 + (y' + b)^2} = \sqrt{b^2 + \Delta^2 + 2b\Delta\sin(\phi)} \tag{A.49}$$

$$\tan\theta = \frac{y' + \Delta}{x'} = \frac{b\sin\phi + \Delta}{b\cos\phi} \tag{A.50}$$

and

$$\vec{e}_\theta \cdot \vec{e}_\phi = [-\sin\theta, \cos\theta] \cdot [-\sin\phi, \cos\phi] = \cos(\theta - \phi) \tag{A.51}$$

In eq. A.5 $\vec{\boldsymbol{dl}} = bd\theta\vec{\boldsymbol{e}}_{\boldsymbol{\phi}}$, and the mutual inductance may after some manipulation be expressed as:

$$M = \frac{2\mu_0 ab}{\pi}\int_0^{\pi} d\phi \frac{b + \Delta\cos\phi}{\rho\beta}\Gamma(m) \tag{A.52}$$

, where we have used the fact that because of symmetry we only need to integrate from 0 to π. Here we have defined (similar to the axial case):

$$\alpha^2 = (a-\rho)^2 + z^2) \tag{A.53}$$

$$\beta^2 = (a+\rho)^2 + z^2) \tag{A.54}$$

$$\Gamma(m) = \frac{(2-m^2)K(m) - 2E(m)}{m^2} \tag{A.55}$$

$$m^2 = 1 - \frac{\alpha^2}{\beta^2} \tag{A.56}$$

It has not so far been possible to find an exact analytic expression for M from eq. A.52 and we have had to integrate it numerically. We have calculated the mutual inductance as a function of lateral displacement for several distances from the transmitter. The results are shown in

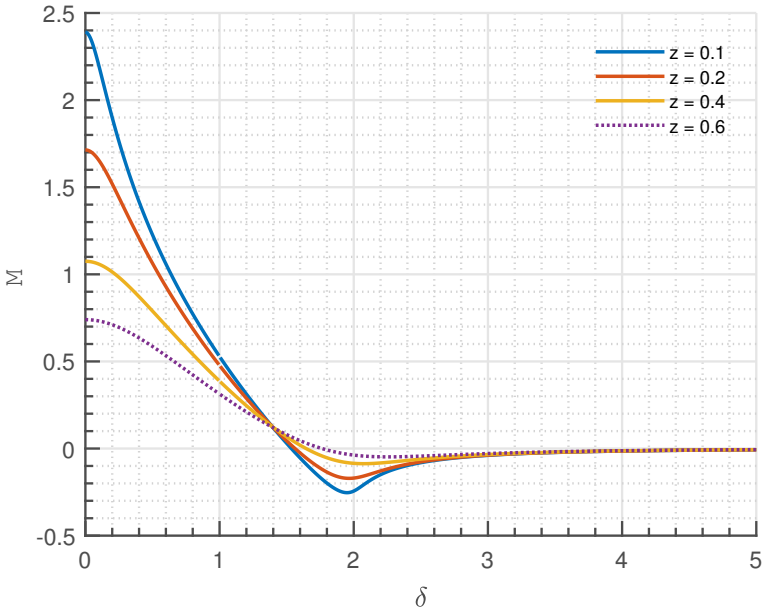

Figure A.12: Mutual inductance between two coaxial, equal sized coils as a function of lateral separation for axial distances $z = 0.1a, 0.2a, 0.4a, 0.6a$

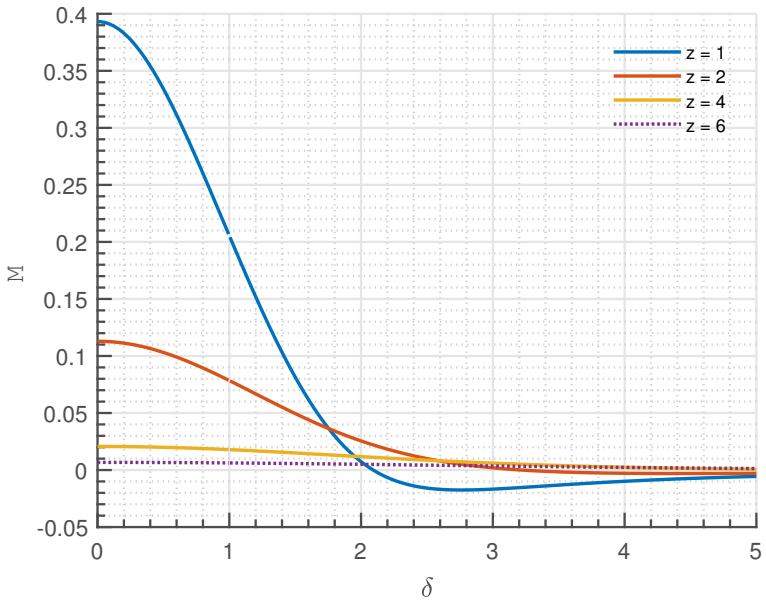

Figure A.13: Mutual inductance between two coaxial, equal sized coils as a function of lateral separation for axial distances $z = a, 2a, 4a, 6a$

A.4 Complete Elliptic Integrals - Definitions and useful formulas

Complete elliptic integrals are extensively used for calculating magnetic fields from circular loops. A number of the various representations and transformations of elliptic integrals used in this thesis is listed here for convenience. For more details see (4). The complete elliptic integral of first kind is defined as

$$K(m) = \int_0^{\frac{\pi}{2}} \frac{dx}{\sqrt{1 - m^2 sin^2 x}} = \int_0^{\frac{\pi}{2}} \frac{dx}{\sqrt{1 - m^2 cos^2 x}} \tag{A.57}$$

and the complete elliptic integral of second kind (Gradstheyn 8.111-3, 8.112-2) is

$$E(m) = \int_0^{\frac{\pi}{2}} \sqrt{1 - m^2 sin^2 x} dx = \int_0^{\frac{\pi}{2}} \sqrt{1 - m^2 cos^2 x} dx \tag{A.58}$$

The two functions are plotted in figure A.14. It is seen that $K(m)$ is strictly increasing function over m, while $E(m)$ is strictly decreasing. $E(m)$ is finite for $0 \leq m \leq 1$, while $K(m)$ is singular for m=1 (a logaritmic singularity).

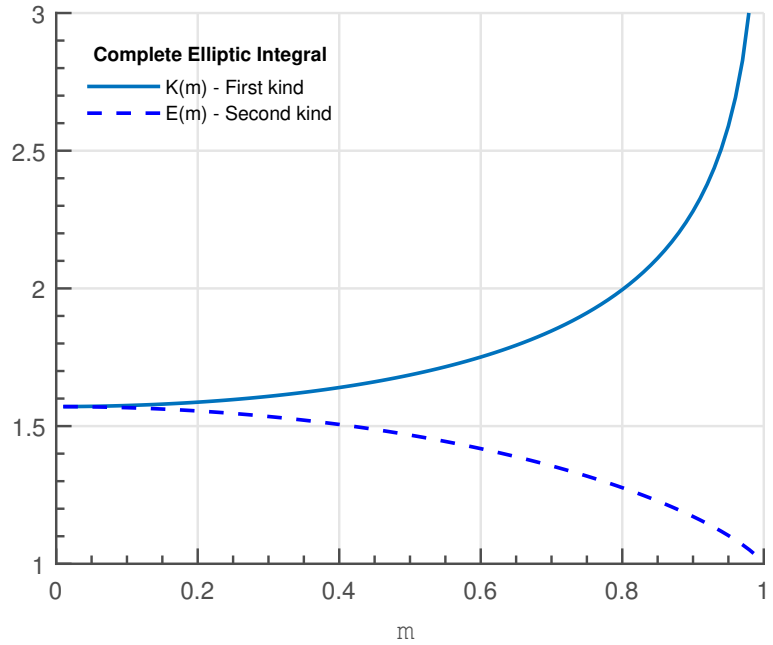

Figure A.14: Complete Elliptic Integrals of First and Second Order

Since

$$\int_0^{2\pi} f(sin^2 x) dx = 2 \int_0^{\pi} f(sin^2 x) dx = 4 \int_0^{\frac{\pi}{2}} f(sin^2 x) dx \tag{A.59}$$

for any regular function f(x), it follows that it doesn't matter which quadrant the integration i (20) is taken over, and for instance

$$K(m) = \frac{1}{4}\int_0^{2\pi} \frac{dx}{\sqrt{1-m^2 sin^2 x}} \tag{A.60}$$

and so on.
Two other useful integral related to complete elliptic integrals are:

$$\int_0^{\frac{\pi}{2}} \frac{dx}{\sqrt{1+m^2 sin^2 x}} = \int_0^{\frac{\pi}{2}} \frac{dx}{\sqrt{1+m^2-m^2 cos^2 x}} = \frac{1}{\sqrt{1+m^2)}} K(\frac{m}{\sqrt{1+m^2}}) \tag{A.61}$$

and

$$\int_0^{\frac{\pi}{2}} dx\sqrt{1+m^2 sin^2 x} = \sqrt{1+m^2)}E(\frac{m}{\sqrt{1+m^2}}) \tag{A.62}$$

Finally, combining these integrals we get

$$\begin{aligned}
\int_0^{2\pi} \frac{dx}{\sqrt{a+bcosx}} &= \int_0^{2\pi} \frac{dx}{\sqrt{a+b-2bsin^2\frac{x}{2}}} \\
&= 2\int_0^{\pi} \frac{dy}{\sqrt{a+b-2bsin^2 y}} \\
&= \frac{2}{\sqrt{a+b}}\int_0^{\pi} \frac{dy}{\sqrt{1-\frac{2b}{a+b}sin^2 y}} \\
&= \frac{4}{\sqrt{a+|b|}} K(\sqrt{\frac{2|b|}{a+|b|}})
\end{aligned} \tag{A.63}$$

and

$$\begin{aligned}
\int_0^{2\pi} \sqrt{a+bcosx}dx &= 2\sqrt{a+b}\int_0^{\pi} \sqrt{1-\frac{2b}{a+b}sin^2 y dy} \\
&= 4\sqrt{a+|b|}E(\sqrt{\frac{2|b|}{a+|b|}})
\end{aligned} \tag{A.64}$$

We have only proved (26) and (27) for $b \geq 0$. However it is easy to verify the two formulas for $b < 0$.

The last integral we need is:

$$\begin{aligned}\int_0^{2\pi} \frac{cosx}{\sqrt{c-dcosx}}dx &= \int_0^{2\pi} \frac{-\frac{1}{d}(c-dcosx)+\frac{c}{d}}{\sqrt{c-dcosx}}dx \\ &= -\frac{1}{d}\int_0^{2\pi}\sqrt{c-dcosx}dx + \frac{c}{d}\int_0^{2\pi}\frac{1}{\sqrt{c-dcosx}}dx \\ &= \frac{4c}{d\sqrt{c+d}}K(\sqrt{\frac{2d}{c+d}}) - \frac{4\sqrt{c+d}}{d}E(\sqrt{\frac{2d}{c+d}}) - \end{aligned} \tag{A.65}$$

To calculate the magnetic field from the vector potential we need to differentiate the compete elliptic integrals. From Gradshteyn 8.123:

$$\frac{dK(m)}{m} = \frac{E(m)}{m(1-m^2)} - \frac{K(m)}{m} \tag{A.66}$$

$$\frac{dE(m)}{m} = \frac{E(m)-K(m)}{m} \tag{A.67}$$

For $m < 1$ it can be shown from eq.(33) and eq. (34) that the series representation is valid:

$$K(m) = \frac{\pi}{2}\sum_{n=0}^{\infty}\left[\frac{(2n)!}{2^{2n}(n!)^2}\right]^2 m^{2n} \tag{A.68}$$

$$E(m) = \frac{\pi}{2}\sum_{n=0}^{\infty}\frac{1}{1-2n}\left[\frac{(2n)!}{2^{2n}(n!)^2}\right]^2 m^{2n} \tag{A.69}$$

The first few terms in eq. A.68 and A.69 is:

$$K(m) = \frac{\pi}{2}\left[1+\frac{1}{4}m^2+\frac{9}{64}m^4+O(m^6)\right] \tag{A.70}$$

$$E(m) = \frac{\pi}{2}\left[1-\frac{1}{4}m^2-\frac{3}{64}m^4+O(m^6)\right] \tag{A.71}$$

In figure A.15, we have plotted the relative error by using a 1, 2 or 3 term approximation instead of the exact expression for K(m) and E(m) (keeping only the first constant term is not considered as an expansion here). It is seen from the figure that for $m < 0.45$ the relative error when retaining only the leading non-trivial term is less than 5. However, for larger m, retaining only one term is less useful.Moreover, for linear combinations of the two elliptic integrals the error may be considerably larger and has to be checked.

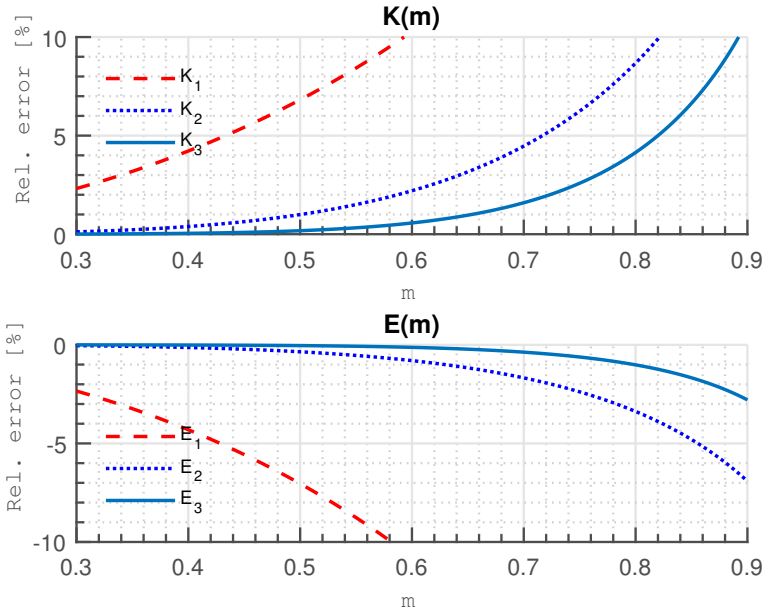

Figure A.15: Relative error for 2 to 4 term approximation of $K(m)$ and $E(m)$, K_n is the n-term approximation to $K(m)$

From Bateman we have the two following transformations that will be useful

$$K\left[\frac{1-k'}{1+k'}\right] = \frac{1+k'}{2}K(k) \tag{A.72}$$

$$E\left[\frac{1-k'}{1+k'}\right] = \frac{E(k)+k'K(k)}{1+k'} \tag{A.73}$$

,where

$$k' = \sqrt{1-k^2} \tag{A.74}$$

Rewriting equation A.72 and combining eq. A.72 and A.73;

$$K(k) = \frac{2}{1+k'}K\left[\frac{1-k'}{1+k'}\right] \tag{A.75}$$

$$E(k) = (1+k')E\left[\frac{1-k'}{1+k'}\right] - \frac{2k'}{1+k'}K\left[\frac{1-k'}{1+k'}\right] \tag{A.76}$$

Appendix B

Transfer functions for SS compensated IPT systems

We will in this chapter derive the frequency characteristics for an SS compensated inductive power transfer (IPT) system.The discussion given here is based on Guidi (17) and Guidi and Suul (18), who has derived the transfer function for the loss-less case, and discusses the lossy case but didn't provide the transfer functions for it.

All IPT systems operating in resonant mode requires tuned circuitry in both receiver and sending circuits. SS compensation means that both sending and receiving circuits has series compensation, and this is the case that will be discussed here. For the other three combination of series and paralell compensation, the reader is referred to Wang et al. (29).

In this appendix, we first derive the circuit equations and the transfer functions. Then we derive the frequency response for two cases:

- Resistive load
- Constant voltage load

B.1 Circuit equations

In this appendix, we have chosen to use p and s as subscripts for the primary (sending) and secondary (pickup) circuit, respectively. This is the convention that is most common in literature. It should be noted however, that in in some of the papers cited, p and s is used as subscript for pickup and sending circuits, respectively, which may sometimes be a bit confusing. In deriving the frequency characteristics we will use Laplace transform, and use $s = j\omega$ to convert the result to frequency. Figure B.1 shows a simplified topology

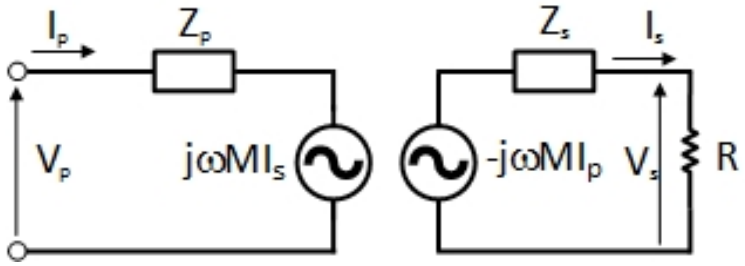

Figure B.1: Circuit topology for an IPT circuit

for an IPT circuit.

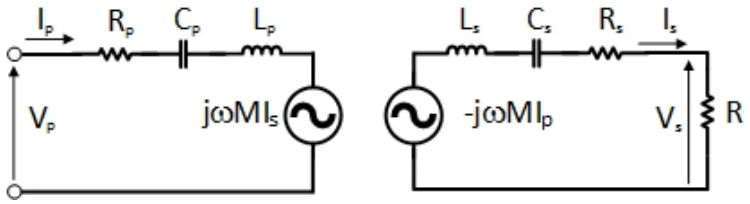

Figure B.2: Circuit topology for series compensated primary and secondary circuit

Figure B.2 shows an SS-IPT compensated circuit, where M is the mutual inductance between the two circuits. The voltage equation for the primary circuit is

$$v_p - Z_p i_p + sMi_s = 0 \tag{B.1}$$

The primary circuit impedance may be expressed as

$$Z_p = \frac{1}{sC_p}\{\frac{s^2}{\omega_p^2} + 2\zeta_p \frac{s}{\omega_p} + 1\} \tag{B.2}$$

Here the standard symbols are used

$$\begin{aligned} &\text{Resonance frequency} && \omega_p = \frac{1}{\sqrt{L_p C_p}} \\ &\text{Damping factor} && \zeta_p = \frac{\omega_p R_p C_p}{2} \\ &\text{Q factor} && Q_p = \frac{1}{\zeta_p} \end{aligned} \tag{B.3}$$

The voltage equations for the secondary circuit are

$$sMi_p - Z_s i_s - v_s = 0 \tag{B.4}$$

where the secondary circuit impedance is

$$Z_s = \frac{1}{sC_s}\{\frac{s^2}{\omega_s^2} + 2\zeta_s\frac{s}{\omega_s} + 1\} \tag{B.5}$$

, with

$$\begin{aligned} &\text{Resonance frequency} && \omega_s = \frac{1}{\sqrt{L_s C_s}} \\ &\text{Damping factor} && \zeta_s = \frac{\omega_s R_s C_s}{2} \\ &\text{Q factor} && Q_s = \frac{1}{\zeta_s} \end{aligned} \tag{B.6}$$

The last equation needed is

$$v_s = Ri_s \tag{B.7}$$

where R is the load resistance.
It is convenient to rewrite the circuit equations in terms of a normalized frequency:

$$Z_p = \frac{1}{\frac{s}{\omega_s}\omega_s C_p}\{(\frac{\omega_s}{\omega_p})^2(\frac{s}{\omega_s})^2 + 2\zeta_p(\frac{\omega_s}{\omega_p})(\frac{s}{\omega_s}) + 1\}$$

$$Z_s = \frac{1}{\frac{s}{\omega_s}\omega_s C_s}\{(\frac{s}{\omega_s})^2 + 2\zeta_s(\frac{s}{\omega_s}) + 1\}$$

$$v_p - Z_p i_p + M\omega_2(\frac{s}{\omega_s})i_s = 0$$

$$M\omega_s(\frac{s}{\omega_s})i_p - Z_s i_s - v_s = 0$$

From now on we will let $\frac{s}{\omega_2} \to s$ whenever it is evident from the context that we operate with normalized frequencies. The final set of circuit equations are then:

$$Z_p = \frac{1}{s\omega_s C_p}\{\eta^2 s^2 + 2\zeta_p \eta s + 1\} \tag{B.8}$$

$$Z_s = \frac{1}{s\omega_s C_s}\{s^2 + 2\zeta_s s + 1\} \tag{B.9}$$

$$v_p - Z_p i_p + M\omega_s s i_s = 0 \tag{B.10}$$

$$M\omega_s s i_p - Z_s i_s - v_s = 0 \tag{B.11}$$

$$v_s = \frac{2\zeta}{\omega_s C_s} i_s \tag{B.12}$$

, where

$$\zeta = \frac{R\omega_s C_s}{2} \tag{B.13}$$

$$\eta = \frac{\omega_s}{\omega_p} \tag{B.14}$$

If one prefers the frequency domain, the conversion is easily made by introducing $s = jw$ into eq. B.6-B.10.

B.1.1 Transfer functions

For analyzing inductive power transfer we write down some of the transfer functions that might be useful. By using eq. B.14 to eliminate v_p from eq. B.11 we get the **transfer function from primary current to secondary current**:

$$G_{i,ss} = \frac{i_s}{i_p} = \frac{M\omega_s s}{Z_s + \frac{2\zeta}{\omega_s C_s}} \tag{B.15}$$

By using the last identity in B.15 to eliminate i_p from B.10 we get the **primary impedance**

$$Z_{pt} = \frac{v_p}{i_p} = Z_p - \frac{M^2\omega_s^2 s^2}{Z_s + \frac{2\zeta}{\omega_s C_s}} \tag{B.16}$$

which is the impedance seen from the primary circuit. This may be expressed as

$$Z_{pt} = Z_p + Z_r \tag{B.17}$$

, where the **reflected impedance** is:

$$Z_r = -\frac{M^2\omega_s^2 s^2}{Z_s + \frac{2\zeta}{\omega_s C_s}} \tag{B.18}$$

The last transfer function we need is the **transfer function from primary voltage to secondary voltage**:

$$\begin{aligned} G_{v,ss} &= \frac{v_s}{v_p} = \frac{R i_s}{Z_{pt} i_p} \\ &= \frac{R}{Z_{pt}} G_{i,ss} \end{aligned} \tag{B.19}$$

The **complex power transferred to the load** is

$$\begin{aligned} S_l &= v_s i_s^* = \frac{v_s v_s^*}{R} \\ &= \frac{G_{v,ss} G_{v,ss}^*}{R} |v_p|^2 \end{aligned} \tag{B.20}$$

The **complex power transferred to the secondary circuit** is

$$\begin{aligned} S_p &= v_r i_p^* = Z_r i_p i_p^* \\ &= \frac{Z_r}{Z_{pt} Z_{pt}^*} |v_p|^2 \end{aligned} \tag{B.21}$$

The **power transferred to the secondary circuit** is thus

$$\begin{aligned} P_p &= Re(Z_r) i_p i_p s^* \\ &= Re(Z_r) \frac{|v_p|^2}{|Z_{pt}|^2} \end{aligned} \tag{B.22}$$

B.2 Resistive Load

B.2.1 Transfer functions

The current-to-current transfer function for the case of purely resistive load is given by eq. B.15:

$$\begin{aligned} G_{i,ss} &= \frac{i_s}{i_p} \\ &= \frac{M \omega_s^2 C_s s^2}{s^2 + 2(\zeta_s + \zeta)s + 1} \end{aligned} \tag{B.23}$$

The reflected impedance follows from eq. B.18:

$$\begin{aligned} Z_r &= -\frac{M^2 \omega_s^2 s^2}{Z_s + \frac{2\zeta}{\omega_s C_s}} \\ &= -\frac{M^2 \omega_s^3 C_s s^3}{s^2 + 2(\zeta_s + \zeta)s + 1} \end{aligned} \tag{B.24}$$

The expression for the sending impedance, eq. B.16, is a bit more complicated than the two previous expressions:

$$\begin{aligned} Z_{pt} &= Z_p - \frac{M^2\omega_s^2 s^2}{Z_s + \frac{2\zeta}{\omega_s C_s}} \\ &= \frac{Z_p(Z_s + \frac{2\zeta}{\omega_s C_s}) - M^2\omega_s^2 s^2}{Z_s + \frac{2\zeta}{\omega_s C_s}} \\ &= \frac{[\eta^2 s^2 + 2\zeta_p \eta s + 1][s^2 + 2(\zeta_s + \zeta)s + 1] - \eta^2 k^2 s^4}{s\omega_s C_p[s^2 + 2(\zeta_s + \zeta)s + 1]} \end{aligned} \tag{B.25}$$

, where we have used that

$$M^2\omega_s^4 C_p C_s = \omega_s^4 k^2 L_s L_p C_p C_s = \omega_s^4 k^2 \frac{1}{\omega_s^2}\frac{1}{\omega_p^2} = \eta^2 k^2 \tag{B.26}$$

By expanding the nominator in eq.B.25 and introducing

$$\zeta_T = \zeta_s + \zeta \tag{B.27}$$

we finally get

$$Z_{pt} = \frac{\eta^2(1-k^2)s^4 + 2\eta[\zeta_p + \eta\zeta_T]s^3 + [\eta^2 + 1 + 4\zeta_p\zeta_T]s^2 + 2[\eta\zeta_p + \zeta_T]s + 1}{s\omega_s C_p[s^2 + 2\zeta_T s + 1]} \tag{B.28}$$

B.2.2 Lossless case

We now consider the lossless case, $\zeta_p = \zeta_s = 0$, with equal primary and secondary circuit resonance frequencies, $\eta = 1$. In this case, the sending impedance is:

$$\begin{aligned} Z_{pt} &= \frac{(1-k^2)s^4 + 2\zeta s^3 + 2s^2 + 2\zeta s + 1}{s\omega_s C_p[s^2 + 2\zeta s + 1]} \\ &= \frac{(s^2+1)[(s^2+1)^2 - k^2 s^4 - 4\zeta^2 s^2] + 2\zeta k^2 s^5}{s\omega_s C_p[(s^2+1)^2 - 4\zeta^2 s^2]} \end{aligned} \tag{B.29}$$

Converting to frequency ($s = jw$):

$$Z_{pt} = \frac{2\zeta k^2\omega^5 - j(1-\omega^2)[(1-\omega^2)^2 - k^2\omega^4 + 4\zeta^2\omega^2]}{\omega\omega_s C_p[(1-\omega^2)^2 + 4\zeta^2\omega^2]} \tag{B.30}$$

From this result it is clear that the reactive part of the sending impedance is zero for $\omega = 1$, which is wanted. However, there may potentially be four more zeros for the reactive part of the sending impedance. These possible zeros is the solution of the equation:

$$(1-\omega^2)^2 - k^2\omega^4 + 4\zeta^2\omega^2 = 0 \tag{B.31}$$

and expanded

$$(1-k^2)\omega^4 - 2(1-2\zeta^2)\omega^2 + 1 = 0 \tag{B.32}$$

This may be written as:

$$\begin{aligned}(1-k^2)(\omega^4 - 2\frac{1-2\zeta^2}{1-k^2}\omega^2 + \frac{(1-2\zeta^2)^2}{(1-k^2)^2}) - \frac{(1-2\zeta^2)^2}{1-k^2} + 1 &= 0 \\ (1-k^2)(\omega^2 - \frac{1-2\zeta^2}{1-k^2})^2 - \frac{(1-2\zeta^2)^2}{(1-k^2)} + 1 &= 0\end{aligned} \tag{B.33}$$

This equation has real solutions only if

$$1 - \frac{1-2\zeta^2}{1-k^2} < 0 \tag{B.34}$$

or

$$\begin{aligned}4\zeta^4 - 4\zeta^2 + k^2 &\geq 0 \\ k &\geq 2\zeta\sqrt{1-\zeta^2}\end{aligned} \tag{B.35}$$

For an ideally matched load we have:

$$R = \omega_s k_0 L_s \tag{B.36}$$

where k_0 is the coupling coefficient for which the system is optimized. Since

$$\zeta = \frac{1}{2}\omega_s R C_s = \frac{1}{2}\omega_s C_s \omega_s k_0 L_s = \frac{1}{2}k_0 \tag{B.37}$$

we get from eq. B.35:

$$k \geq k_0\sqrt{1 - \frac{k_0^2}{4}} \tag{B.38}$$

, which is the requirement for imaginary part of the sending impedance having three zeroes.

B.3 Constant Voltage Load

B.3.1 Transfer functions

We will now consider a system in which the load voltage is constant. The load can not be modelled as an equivalent constant resistance, and although the functional relationship between output current and output voltage can be modelled as

$$v_s = Ri_s \tag{B.39}$$

R will now depend both on frequency and also on the load voltage. The phase of the secondary current must be equal to the phase of the secondary voltage, which means that R will be real. We see that if the angle between the current and voltage is zero(in phase), the load is purely real and only active effect is dissipated. We are now seeking an expression for R as a function of supply and load voltages. By eliminating i_p in eq. (B.10), we get:

$$\begin{aligned} v_p &= Z_p i_p - M\omega_s s i_s \\ &= \frac{(Z_p Z_s - M^2\omega_s^2 s^2)i_s + Z_p v_s}{M\omega_s s} \\ &= \frac{[(Z_p Z_s - M^2\omega_s^2 s^2) + RZ_p]v_s}{MR\omega_s s} \end{aligned} \tag{B.40}$$

,which gives

$$M\omega_s R s v_p = [(Z_p Z_s - M^2\omega_s^2 s^2) + RZ_p]v_s \tag{B.41}$$

By multiplying eq. B.42 with its complex conjugated equation ($s \to -s$), we get:

$$-M^2\omega_s^2 R^2 s^2 |v_p|^2 = [Z_p Z_s - M^2\omega_s^2 s^2 + RZ_p][Z_p^* Z_s^* - M^2\omega_s^2 s^2 + RZ_p^*]|v_s|^2$$

and expanding the right-hand side

$$\begin{aligned} -M^2\omega_s^2 R^2 s^2 \frac{|v_p|^2}{|v_s|^2} &= (Z_p Z_s - M^2\omega_s^2 s^2)(Z_p^* Z_s^* - M^2\omega_s^2 s^2) + Z_p Z_p^* R^2 \\ &+ [Z_p(Z_p^* Z_s^* - M^2\omega_s^2 s^2) + Z_p^*(Z_p Z_s - M^2\omega_s^2 s^2)]R \\ &= |Z_p Z_s - M^2\omega_s^2|^2 + |Z_p|^2 R^2 \\ &+ [|Z_p|^2(Z_s + Z_s^*) - M^2\omega_s^2 s^2(Z_p + Z_p^*)]R \end{aligned} \tag{B.42}$$

Rearranging

$$\begin{aligned} -[M^2\omega_s^2 s^2 \frac{|v_p|^2}{|v_s|^2} + |Z_p|^2]R^2 &= |Z_p Z_s - M^2\omega_s^2 s^2|^2 \\ &+ 2R[|Z_p|^2 Re(Z_s) - M^2\omega_s^2 s^2 Re(Z_p)] \end{aligned} \tag{B.43}$$

we finally get

$$\begin{aligned} -[M^2\omega_s^2 s^2\frac{|v_p|^2}{|v_s|^2}+|Z_p|^2]R^2 &= |Z_pZ_s - M^2\omega_s^2 s^2|^2 \\ &+ 2R[|Z_p|^2R_s - M^2\omega_s^2 s^2 R_p] \end{aligned} \quad \text{(B.44)}$$

B.3.2 Lossless case

For the lossless case, $R_s = R_p = 0$, the last term in eq. (B.44) vanishes, and the equation reduces to:

$$-[M^2\omega_s^2 s^2\frac{|v_p|^2}{|v_s|^2}+|Z_p|^2]R^2 = |Z_pZ_s - M^2\omega_s^2 s^2|^2$$

and

$$R = \frac{|Z_pZ_s - M^2\omega_s^2 s^2|}{[-M^2\omega_s^2 s^2\frac{|v_p|^2}{|v_s|^2} - |Z_p|^2]^{\frac{1}{2}}} \quad \text{(B.45)}$$

With

$$Z_p = \frac{1}{\omega_s C_p s}(\eta^2 s^2+1)$$

$$Z_s = \frac{1}{\omega_s C_s s}(s^2+1)$$

, we get

$$\begin{aligned} R &= \frac{|\frac{1}{\omega_s^2 C_p C_s s^2}(\eta^2 s^2+1)(s^2+1) - M^2\omega_s^4 C_p C_s s^4|}{[-M^2\omega_s^2 s^2\frac{|v_p|^2}{|v_s|^2} + \frac{1}{\omega_s^2 C_p^2 s^2}(\eta^2 s^2+1)^2]^{\frac{1}{2}}} \\ &= \frac{|\frac{1}{\omega_s^2 C_p C_s s^2}(\eta^2 s^2+1)(s^2+1) - M^2\omega_s^4 C_p C_s s^4|}{\frac{1}{\omega_s C_s|s|}[M^2\omega_s^4 c_p^2 s^4\frac{|v_p|^2}{|v_s|^2} - (\eta^2 s^2+1)^2]^{\frac{1}{2}}} \\ &= \frac{1}{\omega_s C_s|s|}\frac{|(\eta^2 s^2+1)(s^2+1) - M^2\omega_s^4 C_p C_s s^4|}{[M^2\omega_s^4 c_p^2 s^4\frac{|v_p|^2}{|v_s|^2} - (\eta^2 s^2+1)^2]^{\frac{1}{2}}} \end{aligned} \quad \text{(B.46)}$$

Introducing

$$x_\mu^2 = \frac{L_p}{L_s}\frac{|v_s|^2}{|v_p|^2} \quad \text{(B.47)}$$

, and replacing M with k, we get

$$\begin{aligned} R &= \frac{1}{\omega_s C_s|s|}\frac{|(\eta^2 s^2+1)(s^2+1) - \eta^2 k^2 s^4|}{[\eta^4\frac{k^2}{x_\mu^2}s^4 - (\eta^2 s^2+1)^2]^{\frac{1}{2}}} \\ &= \frac{1}{\omega_s C_s|s|}\frac{|\eta^2(1-k^2)s^4 + (\eta^2+1)s^2+1)|}{[\eta^4(\frac{k^2}{x_\mu^2}-1)s^4 - 2\eta^2 s^2 - 1]^{\frac{1}{2}}} \end{aligned} \quad \text{(B.48)}$$

Since R has to be real, the expression under the root sign has to be nonnegative. With $s = j\omega$ this requires that

$$\begin{aligned}
\eta^4(\frac{k^2}{x_\mu^2} - 1)\omega^4 + 2\eta^2\omega^2 - 1 &> 0 \implies \\
\eta^4\frac{k^2}{x_\mu^2}\omega^4 - \eta^4\omega^4 + 2\eta^2\omega^2 - 1 &> 0 \implies \\
\eta^4\frac{k^2}{x_\mu^2}\omega^4 - (\eta^2\omega^2 - 1)^2 &> 0 \implies \\
(\eta^2\frac{k}{x_\mu}\omega^2 - \eta^2\omega^2 + 1)(\eta^2\frac{k}{x_\mu}\omega^2 + \eta^2\omega^2 - 1) &> 0 \implies \\
\Big[1 - \eta^2(1 - \frac{k}{x_\mu})\omega^2\Big]\Big[(1 + \frac{k}{x_\mu})\eta^2\omega^2 - 1\Big] &> 0
\end{aligned} \tag{B.49}$$

and finally:

$$\frac{1}{\eta\sqrt{1 + \frac{k}{x_\mu}}} < \omega < \frac{1}{\eta\sqrt{1 - \frac{k}{x_\mu}}} \tag{B.50}$$

It is important to remember that the last equation is for the relative frequency. Using $\omega \to \frac{\omega}{\omega_s}$ and $\eta = \frac{\omega_s}{\omega_p}$, we get:

$$\frac{\omega_p}{\sqrt{1 + \frac{k}{x_\mu}}} < \omega < \frac{\omega_p}{\sqrt{1 - \frac{k}{x_\mu}}} \tag{B.51}$$

, which is the range for which operation is possible in the constant voltage case

Appendix C

Matlab code

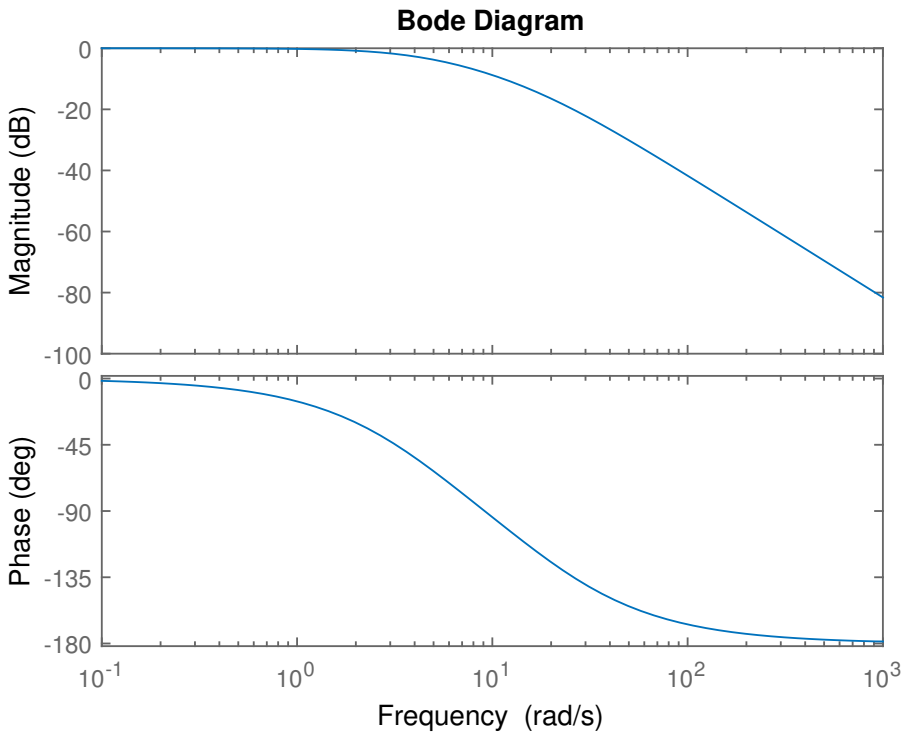

Figure C.1: Bode Plot of H(S)